REVIEW

Research Progress of Hydrostatic Bearing and Hydrostatic-Hydrodynamic Hybrid Bearing in High-End Computer Numerical Control Machine Equipment

Xiaodong Yu[1] · Weicheng Gao[1] · Yanan Feng[1] · Guangqiang Shi[1] · Shihao Li[1] · Minmin Chen[1] · Ruiming Zhang[1] · Junfeng Wang[2] · Wentao Jia[2] · Jianhua Jiao[2] · Ruichun Dai[3]

Abstract

Hydrostatic bearing has the advantages of wide speed range, large bearing capacity, high precision and stability. Hydrostatic-hydrodynamic hybrid bearing can make up for the lack of stiffness of hydrostatic bearing and prevent tribological failure under the condition of high speed and heavy load. Therefore, hydrostatic bearing and hydrostatic-hydrodynamic hybrid bearing have become important bearing parts of high-end computer numerical control (CNC) machine equipment. The research on hydrostatic and hydrostatic-hydrodynamic open a new way for precision improvement of high-end CNC machine equipment. This paper reviews research progress of hydrostatic linear guideway, hydrostatic rest and ram, hydrostatic thrust bearing, hydrostatic-hydrodynamic thrust bearing and hydrostatic-hydrodynamic spindle of high-end CNC machine equipment, and discusses the influence of structure and working parameters on lubrication performance, accuracy and stability of bearing parts. Finally, the future research direction in hydrostatic bearing and hydrostatic-hydrodynamic hybrid bearing are suggested. This review provides a theoretical basis for design and development of high-end CNC machine equipment in the future.

Keywords Hydrostatic bearing · Hydrostatic-hydrodynamic hybrid bearing · Lubrication performance · Working parameter · High-end CNC machine equipment

1 Introduction

In the last decades, hydrostatic bearing has been used in various bearing structures of high-end CNC machine equipment for its advantages of wide speed range, strong bearing capacity, high precision and stability, so as to meet the requirements of high precision, high efficiency, long lifespan and large bearing capacity of CNC machine equipment [1–3]. The hydrostatic bearing hydraulic system supports oil with a certain pressure between two relatively sliding friction pair surfaces, and lubricating oil flow through oil chamber and oil sealing edge, and then flows out from the oil return groove, thus a complete loop is formed. The pressure drop of lubricating oil between oil chamber and oil sealing edge is the source of bearing capacity and stiffness of hydrostatic bearing system. The pressure of oil film in chamber can be regarded as equal pressure distribution, and the pressure of oil film decreases linearly from chamber to oil sealing edge, so the pressure of oil film in the whole chamber can be regarded as a cross-sectional pyramid [4, 5], it is shown in Fig. 1. Hydrostatic bearing structure has the following assumptions under ideal state: hydraulic oil is laminar flow, temperature of hydraulic oil is constant, two relative moving surfaces are absolutely rigid bodies and oil film is incompressible. However, there is obvious defect in studying the deformation of hydrostatic bearing system [6].

Under high speed and heavy load extreme working conditions, temperature of hydrostatic oil film increases, viscosity and stiffness of hydrostatic oil film decreases, which will easily lead to local boundary lubrication or dry friction, and then lead to tribological failure. Hydrodynamic

✉ Xiaodong Yu
yuxiaodong@hrbust.edu.cn

1   Key Laboratory of Advanced Manufacturing and Intelligent Technology, Ministry of Education, Harbin University of Science and Technology, Harbin 150080, China

2   Qiqihar Heavy CNC Equipment Corp. LTD., Qiqihar 161005, China

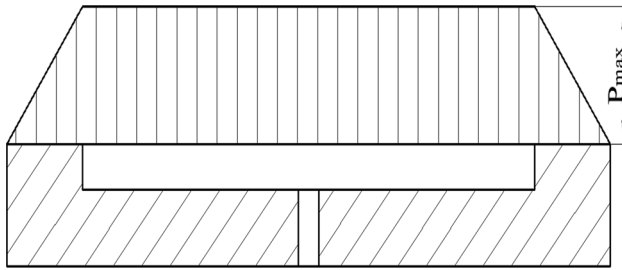3   Qiqihar First Machine Tool Factory Corp. LTD., Qiqihar 161005, China

Fig. 1 Pressure distribution of oil chamber

bearing is added, which can prevent tribological failure caused by high temperature, thus the hydrostatic-hydrodynamic bearing capacity is ensured. Hydrodynamic bearing needs a wedge-shaped gap between two surfaces, and the relative motion speed of two surfaces is high [7]. The pressure distribution of hydrodynamic oil film is shown in Fig. 2. In order to achieve the effect of hydrostatic-hydrodynamic hybrid bearing, parallel gap between two surfaces of friction pair can be changed into wedge-shaped gap on the basis of hydrostatic bearing. For example, traditional hydrostatic thrust bearing can be modified into hydrostatic-hydrodynamic thrust bearing with tilting oil pad. For hydrostatic-hydrodynamic spindle, due to excursion of the center of hydrostatic-hydrodynamic spindle, two friction pair surfaces form angle, and additional hydrodynamic effect appear. This paper illustrates research progress of hydrostatic linear guideway, hydrostatic rest and ram, hydrostatic thrust bearing, hydrostatic-hydrodynamic thrust bearing and hydrostatic-hydrodynamic spindle to enable further development of high-end CNC machine equipment.
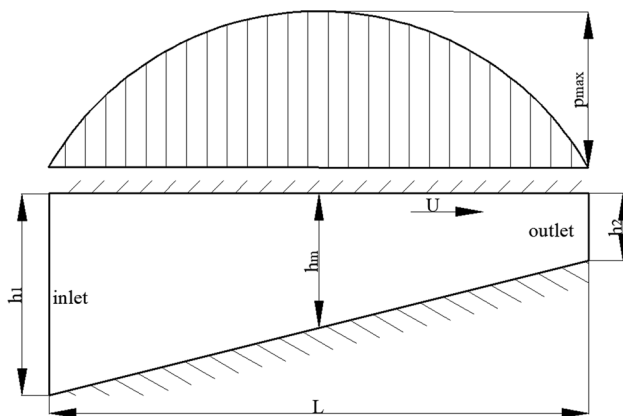
2 Research Progress of Hydrostatic Linear Guideway

Guideway plays the role of bearing and guiding moving parts, its stiffness and moving accuracy directly affect machining accuracy and stability of CNC machine equipment. According to shape, guideway can be divided into linear guideway and circular guideway. According to direction, it can be divided into horizontal guideway and vertical guideway [8, 9]. Hydrostatic bearing can be applied to CNC machine equipment guideway, oil chamber structure and oil film pressure are the key factors that affect stiffness and moving accuracy of hydrostatic guideway [10–12]. Bouzidane et al. [13–15] researched stiffness and damp of hydrostatic guideway. In addition, hydraulic components and oil supply methods also determine the performance of hydrostatic guideway [16]. The form of oil supply of hydrostatic guideway are divided into constant flow oil supply and constant pressure oil supply. Constant flow oil supply is that a amount of lubricating oil is delivered to each oil inlet hole by quantitative pump. The output pressure of oil pump is constant under constant pressure oil supply. Zhang [17] added sensor and proportional pressure valve in constant pressure oil supply system, outlet pressure of valve was changed to adapt different external loads, and thickness of oil film was constant. The diagrams of two forms of oil supply structure are shown in Figs. 3 and 4.
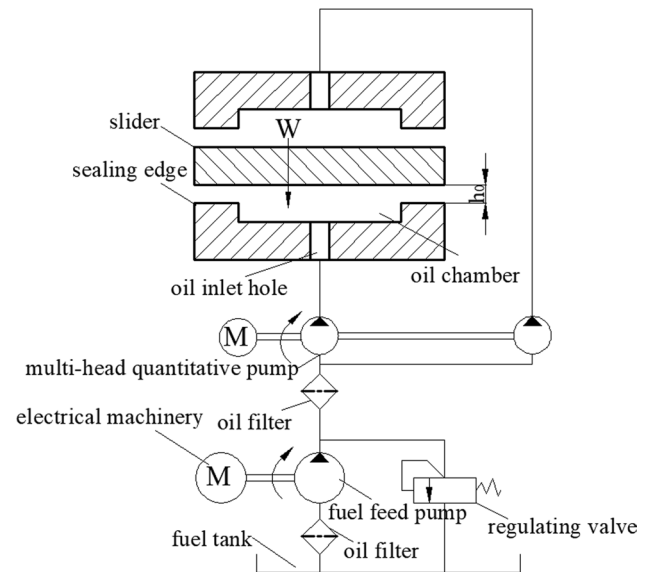

Fig. 2 Pressure distribution of hydrodynamic oil film

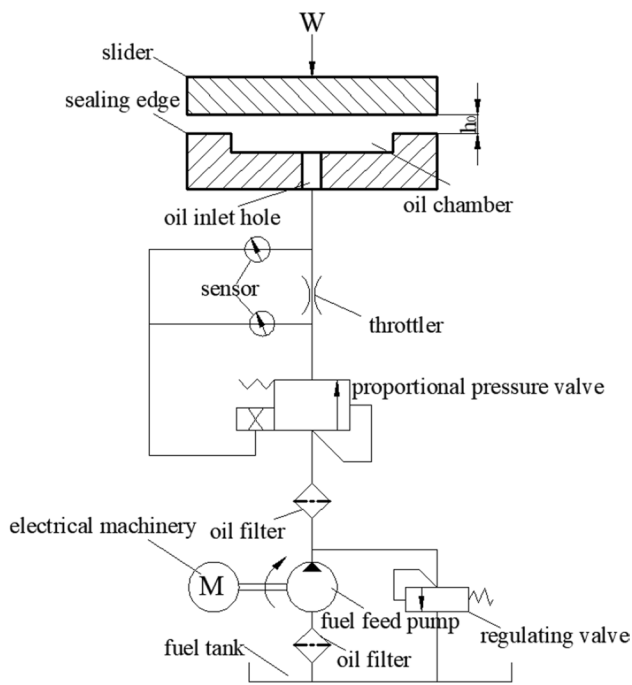**Fig. 3** Schematic diagram of constant flow oil supply structure for hydrostatic guideway

Fig. 4 Schematic diagram of constant pressure oil supply structure for hydrostatic guideway

3 Research Progress of Dynamic Characteristics of Hydrostatic Linear Guideway

Das [18] considered that the damping of machine tool joint accounts for 90% of the damping of the whole machine, some scholars studied the influence of oil film damping on dynamic characteristics of hydrostatic guideway. Wang et al. [19] equated hydrostatic guideway to the system with mass, spring and damper. In order to study the dynamic characteristics of hydrostatic guideway, oil pad of hydrostatic guideway was equivalent to linear spring-damper system and nonlinear spring-damper system. Through step load response and dynamic stiffness experiments, it was found that the calculation accuracy of nonlinear spring-damper system is higher than that of linear spring-damper system. Liu et al. [20, 21] used spring elements to replace stiffness and damping of oil film, and made modal analysis of hydrostatic guideway. The result showed that the first natural frequency of hydrostatic guideway was low, and it was easily interfered by external vibration signals. The finite element model of hydrostatic guideway joint is shown in Fig. 5. Wu et al. [22] put a frequency response function method to analyze the influence of excitation frequency on viscous damping of oil film. The results showed that with the increase of excitation frequency, viscous damping of oil film increased nonlinearly, and hydrostatic guideway was not easily disturbed by high excitation frequency.
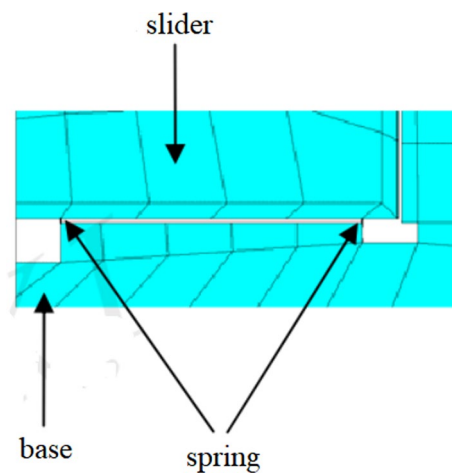

Fig. 5 Finite element model of join part of hydrostatic guideway [20]

Zhao et al. [23, 24] applied hydrostatic bearing to guideway of machine tool beam, and calculated and solved bearing capacity of oil chamber with constant pressure oil supply through principle of vector superposition. The maximum bearing capacity could reach 168.56 kN. At the same time, the dynamic equilibrium equation was established, and the natural frequency of hydrostatic guideway system and the dynamic stiffness of oil film were deduced by squeezing effect of oil film and Taylor expansion, it provided a theoretical basis for the study of dynamic characteristics of hydrostatic guideway. The natural frequency ω_n of hydrostatic guideway system and the dynamic stiffness of oil film j are:

$$\omega_n = \sqrt{\frac{3}{h_0}\left(g + \frac{2P_{i,0}A_e}{m}\right)} \tag{1}$$

$$j = \sqrt{(k - m\omega^2)^2 + c^2\omega^2} \tag{2}$$

where k is static stiffness of oil film, m is slider mass, ω is frequency of external load, c is damp.

Gao et al. [25, 26] analyzed the influence of oil film thickness, oil viscosity and oil supply pressure on the stability of guideway from time domain and frequency domain, the result showed that the stability of hydrostatic guideway would be improved when oil film thickness was small, oil viscosity and oil supply pressure were large in low frequency range, and established kinematics equation and flow equation of closed hydrostatic guideway, and found that flow control valve could improve the dynamic characteristics of hydrostatic guideway. Based on the elastic deformation equation and the dynamic balance equation, Wang et al. [27] established the model of fluid structure interaction of closed hydrostatic guideway of ultra-precision machine tools, and analyzed the influence of platen deformation on dynamic

characteristics of guideway, it was found that the deformation of platen would decrease the stiffness of guideway and increase the transition time of step response.

4 Research Progress of Lubrication Performance of Hydrostatic Linear Guideway

Lubrication performance and accuracy of hydrostatic guideway can be improved by adjusting the flow control device. Lai et al. [28] studied the influence of orifice diameter on stiffness of hydrostatic guideway, and found through the experiment that with the orifice diameter changed from 0.2 to 0.15 mm, the maximum deformation of oil film changed from 2.06 to 1.82 nm, and the stiffness changed from 1453 to 1855 N/nm. Zhang [29] compared PM flow controller with flow control valve, and analyzed the changes of static parameters such as oil film thickness, oil film pressure and oil film stiffness of hydrostatic guideway, the result showed that hydrostatic guideway with PM flow controller had better static characteristics. Shi et al. [30] analyzed the influence of PM flow controller parameters on motion accuracy of hydrostatic guideway, the results showed that initial flow, specific flow and oil supply pressure of PM flow controller could not affect the position where motion error fluctuate, but could affect its fluctuation range. Du et al. [31] designed the parameters of PM flow controller based on the working conditions of linear guideway of precision surface grinding machine, and improved bearting stiffness of hydrostatic linear guideway.

The deformation of guideway also affect the lubrication performance of hydrostatic linear guideway. Zhang [32] put a modified calculation method, which added the surface force deformation of oil chamber into the equilibrium equation of hydrostatic system, and derived more accurate pressure and thickness of oil film. The revised equilibrium equation of hydrostatic system is:

$$
\frac{3Q\mu A_{e1}}{\left(\frac{l_1}{B_1-b_1}+\frac{b_1}{L_1-l_1}\right)(h_x+\Delta L)^3 \times 60 \times 10^8} - F
$$
$$
= \frac{3Q\mu A_{e2}}{\left(\frac{l_2}{B_2-b_2}+\frac{b_2}{L_2-l_2}\right)(2h_0-h_x-\Delta L)^3 \times 60 \times 10^8}
\tag{3}
$$

where Q is flow rate, μ is dynamic viscosity, A_{ei} is effective bearing area, B_i, b_i, L_i and l_i are size parameter of oil chamber, h_0 is thickness of oil film without load, h_x is thickness of oil film with load, ΔL is surface force deformation of oil chamber.

Guo et al. [33] studied the influence law of oil film thickness change on stiffness of hydrostatic guideway, simulated oil film pressure of ultra-precision grinder guideway, and

analyzed its stiffness. The results showed that when oil film thickness of side slider was 13 μm and oil film thickness of middle slider was 14 μm, the stiffness of oil film was the largest.

5 Research Progress of Structure of Hydrostatic Linear Guideway

Gao et al. [34] considered that the distribution of oil chambers was the key factor that affected the bearing performance of hydrostatic guideway, it was found that single row and three columns were the best oil chamber arrangement scheme. Liu [35] compared the pressure distribution of oil film with and without oil return groove under the same working conditions, and found that oil return groove could reduce the fluctuation of bearing capacity of guideway, thus improved the running accuracy of hydrostatic guideway. Wang [36] used finite element simulation to obtain the deformation of guideway caused by oil film pressure, and considered that the deformation of guideway would obviously affect its movement straightness, and took hydrostatic guideway with four opposing oil pads as the experimental object, horizontal and vertical straightness errors of hydrostatic guideway were measured by laser interferometer, it provided a theoretical basis for the deformation compensation of hydrostatic guideway. Chen et al. [37] designed a series compound throttle closed hydrostatic guideway. The advantage of this hydrostatic guideway was that it had multiple independent throttles, which reduced the mutual influence of pressure between oil chambers. The section view of closed hydrostatic guideway is shown in Fig. 6. Li et al. [38] designed a hydrostatic guideway system with controllable oil film thickness. The thrust plate in this system was the key component of main oil film and auxiliary oil film. The auxiliary oil film controlled main oil film to ensure stiffness
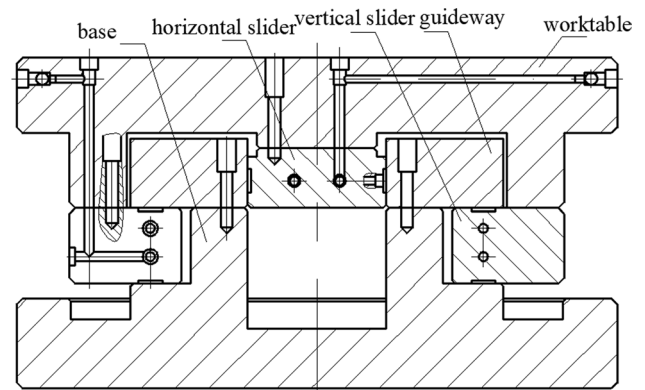

Fig. 6 Section view of closed hydrostatic guideway with series compound throttling [37]

and bearing capacity of hydrostatic guideway. The thrust plate is shown in Fig. 7. According to mathematical model of hydrostatic guideway, Ma and Ran [39] put a relational analysis algorithm, and optimized structural parameters of hydrostatic guideway. Liu et al. [40] designed an oil storage hole in the base of hydrostatic guideway, which could avoid uneven temperature distribution on guideway surface when oil flowed into oil storage hole. Chen et al. [41] designed an sliding assembly of ultra-precision hydrostatic guideway, which improved stability of oil supply through cooperation of oil chamber, tubing, plug plate and fixing pin. Chen et al. [42] put a new type of hydrostatic guideway device, which could make lubricating oil was smoothly delivered to oil inlet hole under the extrusion of spring and top plate. Wu et al. [43] considered that the structure of opposing oil chamber could improve the stability of hydrostatic guideway, and designed hydrostatic guideway with a good anti-torsion performance. For the hydrostatic guideway with large center distance between oil pads, Cha and Li [44] adopted a method to calculate the motion accuracy of hydrostatic guideway with four oil pads. The contour error of guideway surface is fitted by Fourier series, the contour error is:

$$f_z(y) = E \sin(2\pi / \lambda y + \phi) \qquad (4)$$

where E is amplitude, λ is wavelength of contour error, φ is phase angle, y is contour length of guideway surface. According to oil film bearing force and static equilibrium theorem, motion straightness of hydrostatic guideway was deduced. The motion straightness is:

$$e_z = A \cdot B \cdot (f_{e1} + f_{e2} + f_{e3} + f_{e4} - G - W) \qquad (5)$$

where A is structure parameter of sliding, B is matrix of oil film stiffness coefficient, f_{ej} is variation of oil film bearing force of oil pad, G is sliding gravity, W is load.

From the research progress of hydrostatic linear guideway, it can be found that most of research mainly improves lubrication performance and stability of hydrostatic linear guideway by changing flow control device and guideway
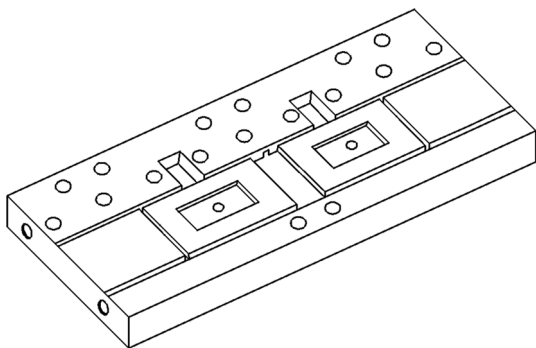
structure, and the main influence factors include: oil supply pressure, oil supply flow, oil film thickness, guideway deformation and working load. In the aspect of deformation compensation of hydrostatic linear guideway, deformation of guideway can be compensated by flow control device or external force. However, there is little research on the modification of hydrostatic linear guideway surface, so according to the deformation law of guideway surface, a shape with equal size and opposite direction can be designed and processed in advance to compensate its elastic deformation.

6 Research Progress of Hydrostatic Rest and Ram

In the cutting process, rest and ram are all affected by cutting force. Therefore, deformation, stiffness and vibration resistance of rest and ram directly affect machining accuracy of CNC machine equipment. Based on the finite element method, the ram of CNC boring and milling machine has been deeply researched [45–47]. For the thermal deformation of ram, Lu et al. [48] analyzed the thermal deformation of ram based on the thermal-structural interaction theory. Li et al. [49] made a comprehensive research on thermal deformation compensation of ram. Mahbubur et al. [50–52] measured force deformation of ram and optimized its structure. At the same time, Liu et al. [53–55] researched deformation compensation methods of ram, such as pull rod compensation method. With the increasing cutting load and machining accuracy, hydrostatic bearing has been applied to rest and ram of CNC machine equipment in recent years.

7 Research Progress of Hydrostatic Rest and Ram of Vertical Lathe

Vertical lathe is used to process heavy parts with small proportion of length and diameter, its rest mainly includes: carriage, ram and tool holder. Cutting process of vertical lathe is shown in Fig. 8. Compared with traditional rest of vertical lathe, hydrostatic rest of vertical lathe has a complete oil supply system and can stand greater cutting force, such as DVT series vertical lathe [56]. After hydrostatic bearing is added to rest, the maximum cutting force can be 6.3t, internal structure, oil chamber and ram of hydrostatic rest of vertical lathe are shown in Figs. 9, 10 and 11.

Yang [57] considered that the change of oil film thickness of hydrostatic rest would cause a certain deflection angle of vertical ram, and took hydrostatic tool rest with constant current oil supply as research object, calculated the total displacement at the bottom of ram was 9.016 μm. Cheng [58] simulated oil film pressure field of single oil chamber and double oil chamber of hydrostatic rest by Fluent, it was
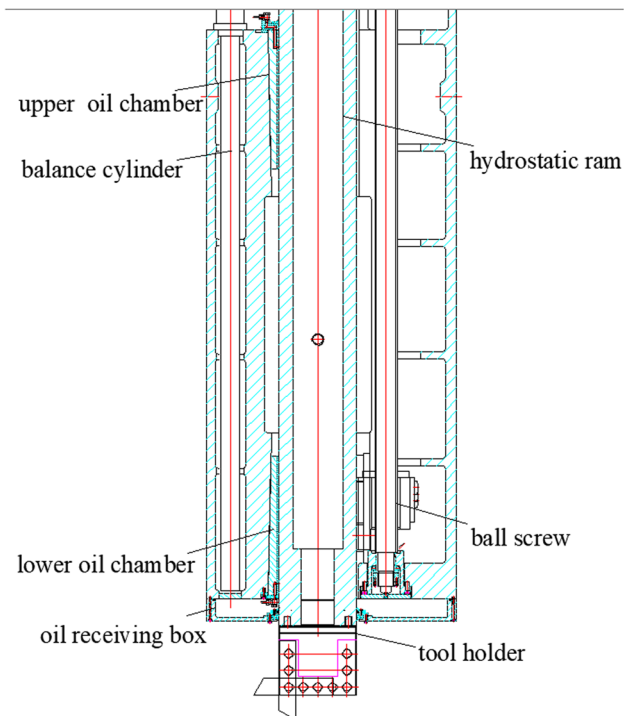

Fig. 7 Thrust plate [38]

Fig. 8 Cutting process of vertical lathe

Fig. 10 Oil chamber of hydrostatic rest of vertical lathe

Fig. 9 Internal structure of hydrostatic rest of vertical lathe

Fig. 11 Hydrostatic ram [56]

found that the bearing performance of double oil chamber was better than that of single oil chamber. The pressure field of hydrostatic rest oil chamber is shown in Fig. 12.

Wang et al. [59, 60] calculated the bearing capacity of a single oil chamber by Reynolds equation, and analyzed nonlinear bearing force and stiffness of two opposing oil chambers by Gauss–Seidel, it was found that with the decrease of oil film thickness, the stiffness of oil film increased, but oil film was easy to crack when oil film thickness was small, and oil film bearing capacity could
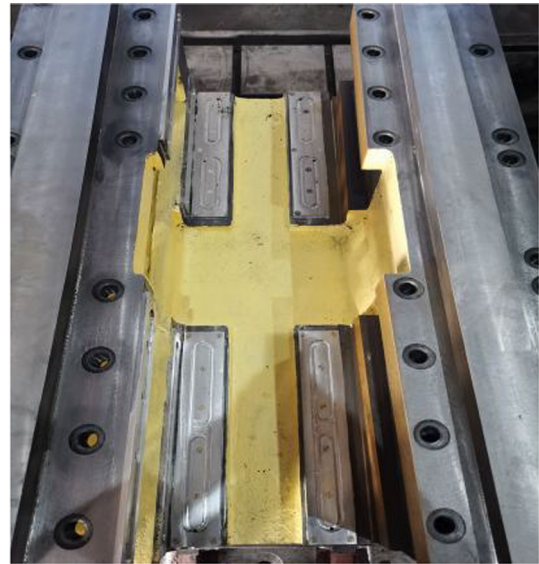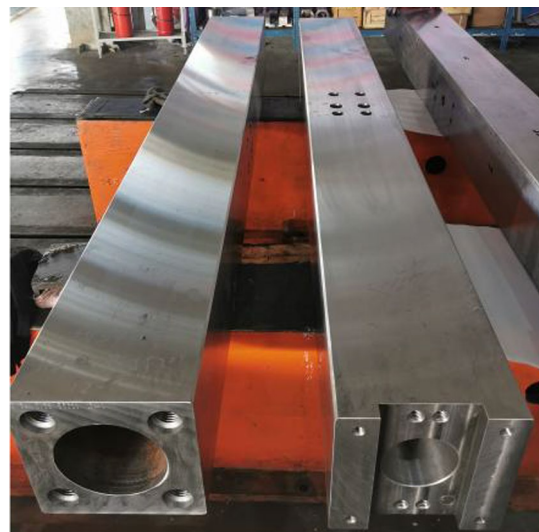
not exceed the maximum pump pressure. Therefore, the gap could appropriately reduce to improve oil film stiffness. At the same time, static and damping components of hydrostatic rest were analyzed, it was found that symmetrical distribution of oil chamber was beneficial to improve static and dynamic characteristics of hydrostatic rest. Zhang et al. [61] put a method to measure the deformation of hydrostatic rest. Under the condition of oil supply, force was added to ram surface by proving ring, and the deformation of hydrostatic ram was read by dial indicator. This method provided a reference for the measure
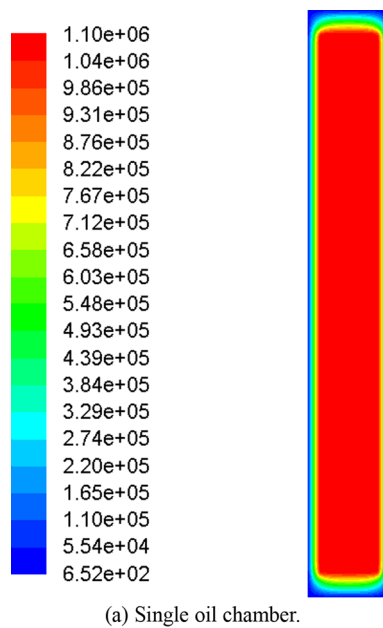
(a) Single oil chamber.
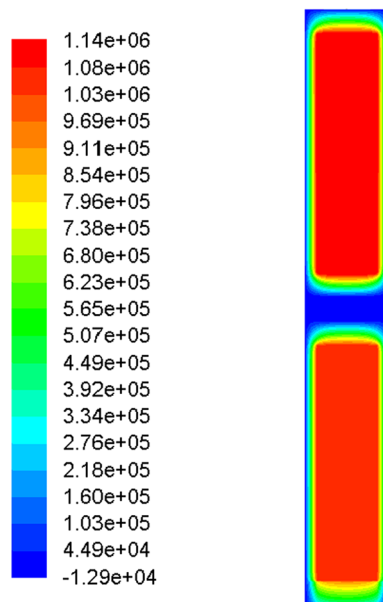
(b) Double oil chamber.

Fig. 12 The pressure field of hydrostatic rest oil chamber [58]

(a) Proving ring.

(b) Position of dial indicator.

Fig. 13 Measure instruments [61]

8 Research Progress of Hydrostatic Rest and Ram of Milling Machining Center

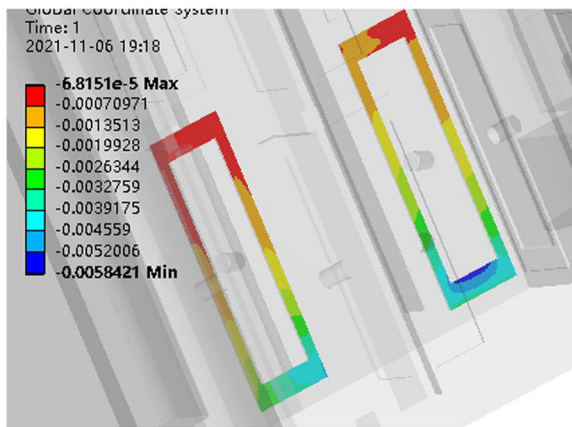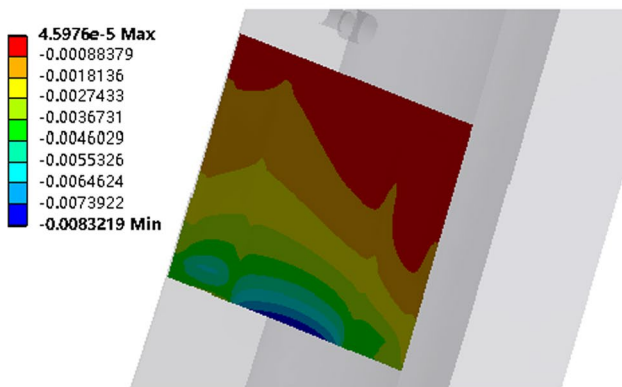Hydrostatic bearing is not only applied to rest and ram of vertical lathe, but also applied to rest and ram of milling machining center. Hydrostatic guideway structure is adopted inside the headstock, which can make ram suspend on oil film for linear movement, and improve bearing capacity of ram and reduce friction [63]. Wu et al. [64] added hydrostatic bearing to compensate deformation of ram of boring and milling machine rest and ram, it could compensate radial bending deformation of ram by increasing or decreasing oil supply pressure of the first group of oil chambers and the second group of oil chambers. The measure of ram bending compensation is shown in Fig. 15. Based on hydrostatic bearing, Zheng [65] put a hydraulic micro-gap compensation system, which could effectively improve the contact stiffness of ram of gantry milling machine and compensate the errors caused by micro-gap. Hua et al. [66, 67] applied opposite hydrostatic oil pad to rest and ram of large floor boring and milling machine, and topology optimized hydrostatic ram structure, which improved bearing capacity, vibration resistance and machining accuracy of large floor boring and milling machine. Oil chamber distribution form of ram of CNC

of deformation and stiffness of hydrostatic rest. Measure instruments are shown in Fig. 13. Gao [62] added pressure field of oil film of hydrostatic rest to ANSYS Workbench, and simulated deformation of hydrostatic rest, obtained deformation distribution of friction pair, and predicted the shape of oil film of hydrostatic rest. The result showed that the deformation of lower part of friction pair was large due to bending deformation of ram. When the ram overhang length is 2 m, the deformation of friction pairs on the lower oil chamber of hydrostatic rest are shown in Fig. 14.

(a) Deformation of oil chamber.

(b) Deformation of ram.

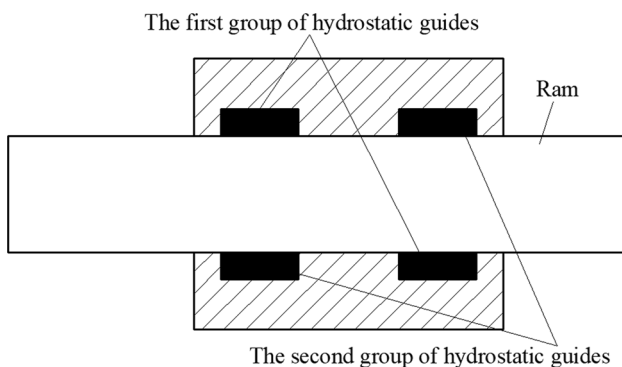**Fig. 14** Deformation of friction pairs [62]

Fig. 15 Measures of bowing compensation of the ram [64]

floor boring and milling machine is shown in Fig. 16, section A and section B of hydrostatic guideway of machine head are shown in Fig. 17.

Gao [68] took GTM500200 turning and milling machining center as research object, designed distribution and parameters of oil chamber of hydrostatic rest,
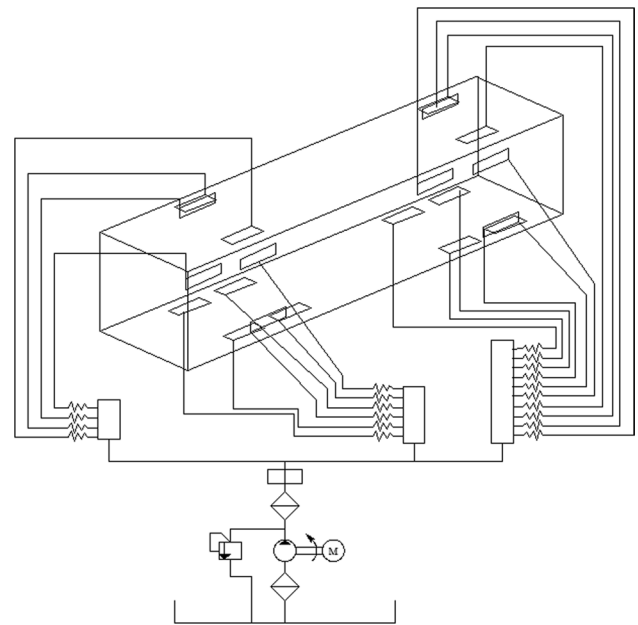

Fig. 16 Distribution form of ram oil chamber of CNC floor boring and milling machine [66]

and calculated pressure, flow rate and stiffness of oil film. These provided theoretical reference for the machining accuracy was improved of turning and milling machining center. Wang and Chen [69] took spindle box of TH6918 boring and milling machining center as the research object, and measured oil film pressure and thickness of hydrostatic guideway under different ram overhang lengths. The measured results provided a theoretical basis for hydrostatic guideway structure was improved. Dong [70] added a compensation oil pad at the bottom of ram to support ram and reduced deflection value of ram of CNC floor boring and milling machine. Yu et al. [71] designed a hydrostatic rolling composite guideway device in the rest of vertical lathe and milling machine, which improved accuracy, moving speed, stiffness, bearing capacity, vibration resistance and wear resistance of rest. The hydrostatic rolling composite guideway device is shown in Fig. 18.

The oil film pressure in hydrostatic rest and ram is obtained by simple force analysis and theoretical calculation. However, there are many oil chambers in hydrostatic rest, and oil film pressure is uneven, at the same time, ram is connected with ball screw, which will also cause additional force. In the cutting process, the force of ram is very complicated. Oil film pressure obtained by simple force analysis is not accurate. Therefore, the actual stress situation of hydrostatic ram should be comprehensively considered, and oil film pressure of hydrostatic ram should be directly or indirectly determined by experimental measurement or elastic model.

opposite oil pad

(a) Section A

Fig. 18 Hydrostatic rolling combination guideway [71]

equipment, hydrostatic thrust bearing has advantages of low friction coefficient, low driving power and long service life [72–74]. Lubricating oil viscosity, oil film thickness, oil film temperature and oil chamber structure all have influences on the performance of hydrostatic thrust bearing [75–77]. Hydrostatic thrust bearing of vertical machining equipment is shown in Fig. 19, and oil supply system of hydrostatic thrust bearing is shown in Fig. 20.
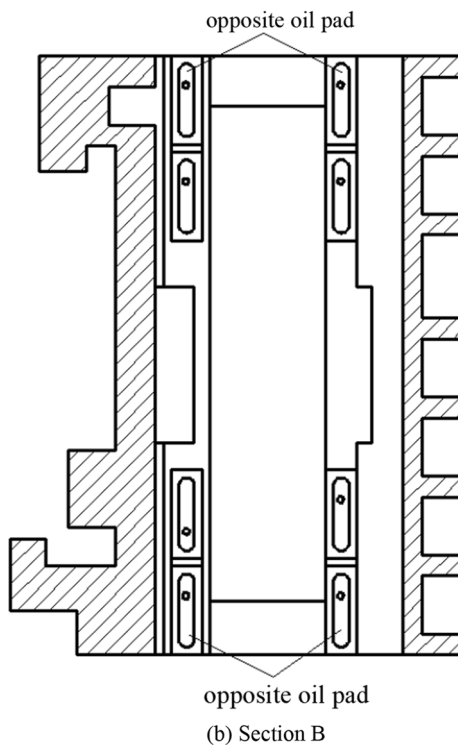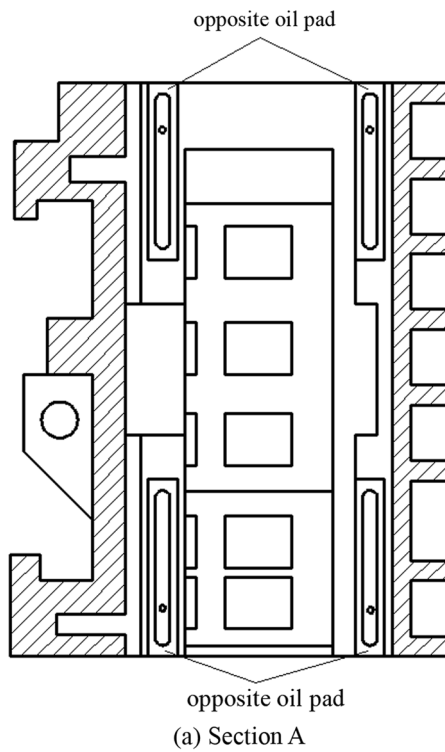
opposite oil pad

(b) Section B

Fig. 17 Section of machine head hydrostatic guideway [67]

9 Research Progress of Hydrostatic Thrust Bearing
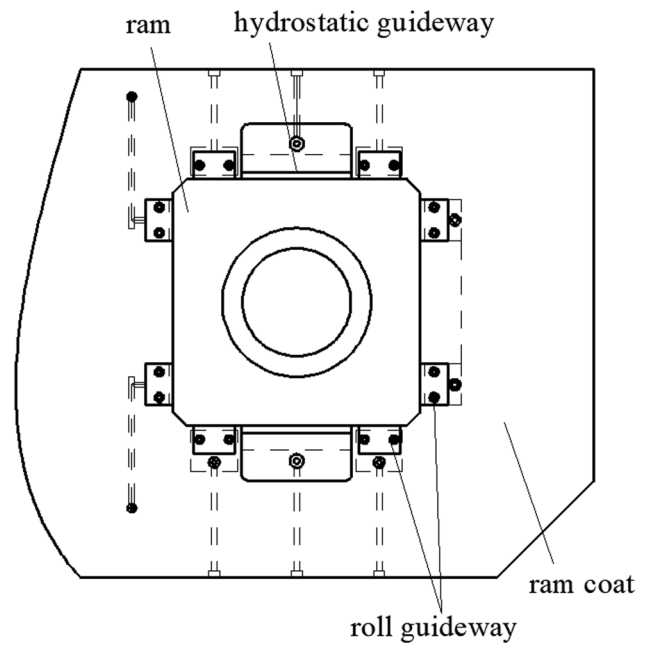
As the core component of large-scale CNC machine

Fig. 19 Hydrostatic thrust bearing
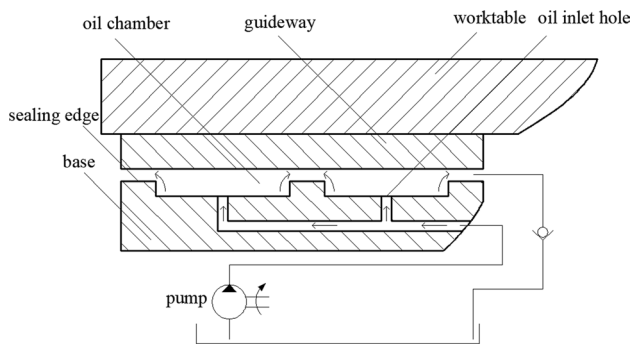
Fig. 20 Internal oil supply system of hydrostatic thrust bearing

Fig. 21 Offset condition diagram [87]

10 Research Progress of Lubrication Characteristics of Hydrostatic Thrust Bearing Oil Film

In the research of oil film bearing capacity, Yu et al. [78] used computational fluid dynamics method to research the pressure distribution of gap fluid of multi-pad annular recess hydrostatic thrust bearing, it was found that with the increase of worktable rotational speed, oil film pressure decreased. Singh et al. [79–81] considered that centrifugal force and inertia would have a certain influence on lubrication performance of oil film of hydrostatic thrust bearing under high speed and heavy load working conditions. According to the influence of inertia force and centrifugal force on the bearing performance of hydrostatic thrust bearing, Yu et al. [82] analyzed the variation law of oil film pressure and oil film thickness, and found that with the increase of rotational speed of worktable, oil film thickness decreased, so centrifugal force could easily cause friction failure of hydrostatic bearing. Wang et al. [83] calculated bearing capacity of hydrostatic thrust bearing with sector chamber and constant flow oil supply under centrifugal force, and established experiment system of heavy hydrostatic turntable, which provided theoretical basis for design and calculation of this kind of hydrostatic thrust bearing. Based on lubrication theory and tribology principle, Yu et al. [84] deduced the relationship between oil film thickness and bearing capacity of multi-pad annular recess hydrostatic thrust bearing under centrifugal force. The relationship is:

$$h = h_0 - \Delta h = h_0 - \sqrt[3]{\frac{3Q_p\mu A_b}{W_0 + W}} - \sqrt[3]{\frac{18\mu\Delta Q_w}{\pi\rho\omega^2 r^2}} \qquad (6)$$

where h_0 is oil film thickness when load is 0t, Q_p is oil inlet flow, μ is dynamic viscosity of lubricating oil, A_b is effective bearing area, W_0 is weight of worktable, W is weight of workpiece, ΔQ_w is flow generated by centrifugal force, ρ is lubricating oil density, ω is angular velocity, r is center distance.
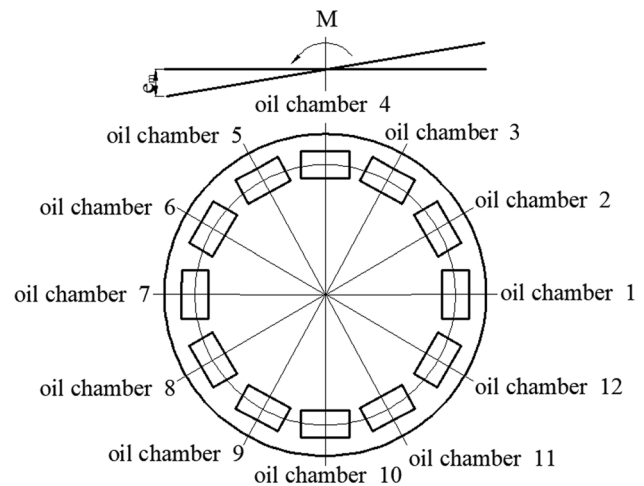
Quan et al. [85] used dynamic grid technology to simulate oil film pressure of hydrostatic thrust bearing under different working conditions. The results showed that the higher inlet velocity, the higher oil film pressure, and due to pressure loss, pressure in chamber decreased with the increase of rotational speed when oil film thickness was small. Rehman et al. [86] put the active control theory to realize the active lubrication of hydrostatic thrust bearings, and improved capacity and stability of hydrostatic bearing. Liu et al. [87] researched the influence of eccentric load distance on bearing performance under offset condition, and derived oil film pressure equation of double rectangular chambers under offset condition. Offset condition diagram is shown in Fig. 21, equations of oil film pressure under offset condition are shown in Table 1.

In the research of oil film temperature rise and flow pattern of hydrostatic thrust bearing, Tan et al. [88] simulated temperature field of hydrostatic thrust bearing with sector chamber under different rotational speeds based on computational fluid dynamics theory, and the result showed that oil film temperature was greatly influenced by rotational speed of worktable. Oil film temperature field under 31.5 rmp and 40 rmp of worktable rotational speed are shown in Fig. 22. From temperature field, it can be found that temperature at oil sealing edge of oil pad is higher, and temperature is higher when the rotational speed was 40.

According to computational fluid dynamics and finite element, Srinivasan [89] analyzed the lubrication characteristics of ultra-heavy constant-flow hydrostatic thrust bearing. The result showed that with the increase of worktable rotational speed, oil film temperature increased. Based on the lubrication theory, Yu et al. [90] simulated flow pattern of oil film in the clearance of hydrostatic thrust bearing. The simulation results showed that with the increase of rotational speed, the flow state in chamber changed from laminar flow

Table 1 Oil film pressure equation

Oil film pressure	Pressure formula under eccentric load
P_1	$\frac{p_0}{1+\varepsilon_m}$
P_2	$\frac{p_0}{1+\frac{\sqrt{3}}{2}\varepsilon_m}$
P_3	$\frac{p_0}{1+\frac{1}{2}\varepsilon_m}$
P_4	p_0
P_5	$\frac{p_0}{1-\frac{1}{2}\varepsilon_m}$
P_6	$\frac{p_0}{1-\frac{\sqrt{3}}{2}\varepsilon_m}$
P_7	$\frac{p_0}{1-\varepsilon_m}$
P_8	$\frac{p_0}{1-\frac{\sqrt{3}}{2}\varepsilon_m}$
P_9	$\frac{p_0}{1-\frac{1}{2}\varepsilon_m}$
P_{10}	p_0
P_{11}	$\frac{p_0}{1+\frac{1}{2}\varepsilon_m}$
P_{12}	$\frac{p_0}{1+\frac{\sqrt{3}}{2}\varepsilon_m}$

Where ε_m is displacement rate under the action of overturning couple moment.

(a) Rotational speed is 31.5rpm.
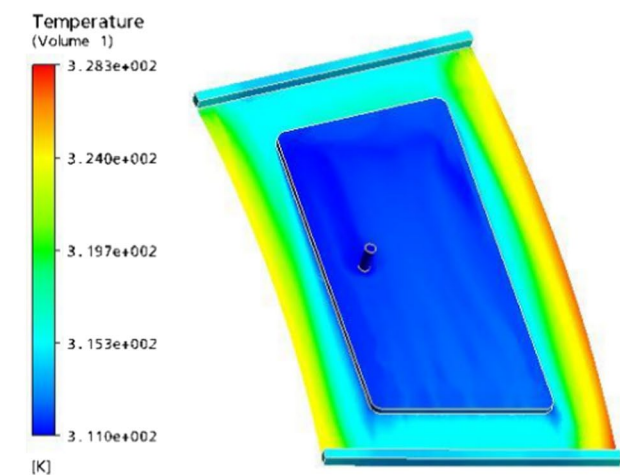
(b) Rotational speed is 40rpm.

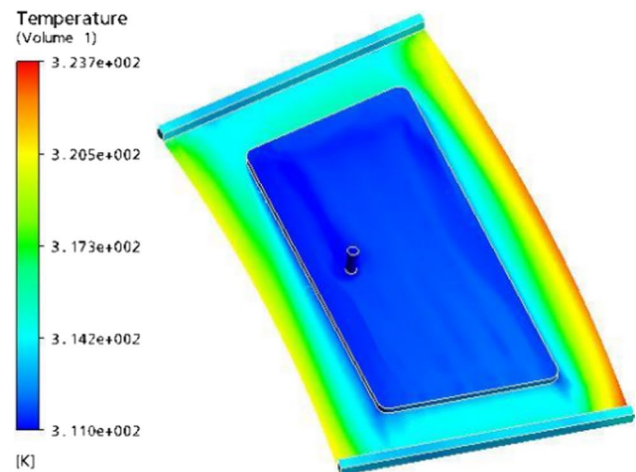**Fig. 22** Temperature of oil film [88]

to turbulent flow, and the turbulent flow became more obvious, and the flow on oil seal edge kept laminar flow. Feng et al. [91, 92] took sector chamber as the research object, put a calculation method of oil film temperature rise with hot oil carrying, established the equation of oil supply temperature rise under the influence of hot oil carrying, and simulated oil film temperature under different working conditions by finite element method. The results showed that when worktable rotated counterclockwise, the hot oil carrying phenomenon occurred in oil sealing edge area on the right side of oil pad, and the hot oil carrying factor was greatly affected by rotational speed, and overall oil film temperature rise increased with the increase of rotational speed and load. The temperature rise equation is as follows:

$$T_0 = T_{in} + \alpha\Delta T \tag{7}$$

where T_{in} is oil inlet temperature of oil chamber, T_0 is oil supply temperature, ΔT is temperature rise on the downstream side sealing edge caused by hot oil carrying, α is hot oil carrying factor, the expression of hot oil carrying factor is:

$$\alpha = \frac{3a\mu\omega(R_1 + R_4) - \Delta p h^2}{3a\mu\omega(R_1 + R_4) + \Delta p h^2} \tag{8}$$

where a is width of oil sealing edge, μ is dynamic viscosity, ω is angular velocity, h is oil film thickness, Δp is pressure difference between oil chamber and oil return groove, R_1

is inner diameter of oil pad rotation center, and R_4 is outer diameter of oil pad rotation center.

Singh et al. [93] researched the viscosity of hydrostatic thrust bearing lubricant. Zhang et al. [94] established a mathematical model of hydrostatic thrust bearing with multi-oil pads under variable viscosity, and found that viscosity of lubricating oil had an important influence on the performance of hydrostatic thrust bearing. Chen [95] used Fluent to simulate pressure field of oil film under different lubricating oil viscosity. The simulation results showed that in order to improve bearing capacity of oil film, when the load of hydrostatic thrust bearing was 40t, HL-15, HL-22 and HL-32 types of lubricating oil should be selected, and when the load was 80t, HL-46 and HL-48 types lubricating oil should be selected. In order to reduce temperature rise of lubricating oil, when the rotational speed of worktable was lower than 20 r/min, HL-46 and HL-68 types of lubricating oil should be selected, and when the rotational speed

of worktable was higher than 20 r/min, HL-15 and HL-22 types of lubricating oil should be selected. Zhang et al. [96, 97] researched the lubrication characteristics of oil film of Q1-205 hydrostatic thrust bearing under variable viscosity and variable load by dynamic grid technology, it was found that the pressure loss on the downstream side of oil chamber seal oil edge was larger. Yu et al. [98] used power exponent function to fit viscosity and temperature of lubricating oil, and deduced the relationship equation of viscosity and temperature, which provided a theoretical basis for the research of the influence of temperature on bearing capacity of oil film. Viscosity-temperature relation equation is:

$$\mu = 3.5665 \times 10^{31}(T_0 + \Delta T)^{-13.22838} \tag{9}$$

where μ is dynamic viscosity, T_0 is initial temperature, ΔT is temperature rise.

11 Research Progress of Oil Chamber Structure of Hydrostatic Thrust Bearing

In order to improve bearing capacity and positioning accuracy and reduce surface friction of large size hydrostatic thrust bearing under high speed and heavy load conditions, many scholars have researched and improved oil chamber structure [99]. Kumar and Sharma [100] considered that geometry and area of oil chamber were the key factors that affect performance of hydrostatic thrust bearing. Chow [101] compared bearing capacity of circular chamber and annular chamber of hydrostatic thrust bearing, and found that annular chamber had stronger bearing capacity. Sharma et al. [102] simulated pressure and temperature fields of different shapes of oil chambers, and found that annular oil chamber had the best comprehensive performance. Heinrichson et al. [103, 104] established the dynamic model of tilting pad thrust bearing, and found that shallow oil chamber could improve performance of bearing, and verified this conclusion by experiment. Yadav et al. [105, 106] put a hydrostatic thrust bearing structure with surface texture, which could reduce friction. Shao et al. [107–110] compared distribution of temperature field and flow field of gap oil film of different shapes and depths of chamber, and optimized the structure of oil chamber. Based on the computational fluid dynamics theory, Wang et al. [111] analyzed the influence of water chamber depth and water inlet diameter on bearing capacity. The result showed that with the increase of water chamber depth or water inlet diameter, bearing capacity first increased and then remained unchanged. Li et al. [112] researched the influence of depth and oil seal edge size of oil chamber on the temperature field of hydrostatic thrust bearing. The result showed that when oil seal edge width was 10 mm

and oil chamber depth was 10 mm, oil film temperature rise was the lowest. Sun [113] took double rectangular oil chamber as the research object, analyzed pressure field, temperature field and velocity field of oil film of different structural sizes of oil chamber, and combined with MATLAB, it was found that the lubrication performance was the best when the area ratio of oil chamber in oil pad was 75%. Xiao el al. [114] analyzed the flow pattern distribution of circular oil chamber with multi-ring structure, and found that the flow pattern of circular oil chamber with multi-ring structure was more stable and the pressure distribution was more uniform. Guo et al. [115] used finite element method to simulate temperature field of rectangular chamber, sector chamber, elliptical chamber, and I-section chamber of hydrostatic thrust bearing, and obtained oil film temperature rise of four chambers with the same area and under the same working conditions. The maximum oil film temperatures of four chambers are shown in Table 2. Shao et al. [116] researched the lubrication characteristics of annular hydrostatic thrust bearings with different groove depths. Through simulation, it was found that the lubrication characteristics were the best when the groove depth was 3.5 mm. Yu et al. [117] simulated pressure field, temperature field and velocity field of oil chambers with different groove shapes. Through comparison, it was found that the lubrication performance of oil chambers with circular grooves was the best. Wang [118] made a comprehensive research on different chamber shapes, chamber depths and sizes of oil inlet holes of hydrostatic thrust bearings, and comprehensively compared pressure field and temperature field of oil film of different chamber structures. It was concluded that the optimal chamber depth of double rectangular oil chamber was 3 mm and the optimal diameter of oil inlet hole was 15 mm, the optimal chamber depth of ring oil chamber was 2.5 mm, and the optimal diameter of oil inlet hole was 15 mm, the optimal chamber depth of circular oil chamber was 3.5 mm, and the optimal diameter of oil inlet hole was 15 mm, the optimal chamber depth of runway oil chamber was 5 mm, and the optimal diameter of oil inlet hole was 14 mm. Tian et al. [119] used the small perturbation method to solve stiffness and damping coefficient of oil film, and the result showed that annular oil chamber was better than circular oil chamber.

Table 2 Maximum temperature of oil film in four oil chamber

Chamber shap	Rectangular chamber	Sector chamber	Elliptical chamber	I-section chamber
Maximum temperature/K	314.0432	314.0836	314.1451	314.1856

12 Research Progress of Fluid–Structure Interaction Deformation of Hydrostatic Thrust Bearing

Under high speed and heavy load working condition, the friction between worktable and oil film generates heat, which leads to thermal deformation and force deformation of hydrostatic bearing. The finite element method can be used to analyze thermal deformation and force deformation of surface [120–122]. Based on theory of fluid–structure interaction, Yang [123] researched the deformation of hydrostatic thrust bearing, through simulation, it was found that the deformation of base was gradient distribution, increased from inside to outside, and the overall deformation of hydrostatic bearing was wedge-shaped with open outward at the lubrication gap. Fu et al. [124] researched the thermal deformation of hydrostatic thrust bearing with annular recess multi-oil pads, and obtained thermal deformation of worktable and base through finite element simulation, it could be found that the maximum thermal deformation of worktable occurred at the bottom of radial outer edge, and the maximum thermal deformation of base occurred at the top of radial outer edge, and the actual shape of oil film was "trumpet" under the combined action of thermal deformation of worktable and base. Ettles et al. [125] analyzed the influence of thermal effect of oil film boundary layer on the bearing performance of hydrostatic thrust bearing, and optimized structure of hydrostatic thrust bearing. Yu et al. [126–128] obtained the deformation of friction pair of hydrostatic thrust bearing by fluid–structure interaction, and found that with the increase of rotational speed of worktable, the increment of deformation of friction pair also increased, and predicted the shape of oil film of hydrostatic bearing. Zheng et al. [129, 130] calculated the heat transfer coefficient of hydrostatic thrust bearing under different working conditions, and simulated overall thermal deformation of worktable and base by ANSYS Workbench, and through experiment verification, the overall thermal deformation characteristics of hydrostatic thrust bearing were obtained, and optimal load of hydrostatic thrust bearing was between 16 and 30t. Deformation of worktable and base is shown in Fig. 23. From Fig. 23, it can be found that deformation of worktable and base increase from the center of rotation to the periphery. Li et al. [131] added a micro-heat pipe structure to the joint of worktable and base of hydrostatic thrust bearing, and numerically simulated the temperature field of oil film and the thermal deformation of worktable and base. The results showed that micro-heat pipe had a good thermal conductivity, could take away most of heat generated by oil film shearing, and effectively control temperature rise and thermal deformation of hydrostatic thrust
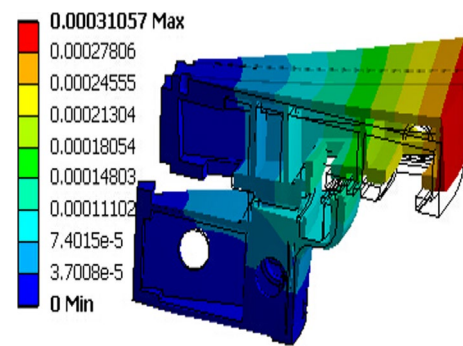

Fig. 23 Deformation of worktable and base [129]

bearing, avoid dry friction, improve processing quality of equipment. Micro heat pipe structure of hydrostatic thrust bearing is shown in Fig. 24.

Most of research focus on the lubrication performance of hydrostatic thrust bearing, but in the operation process, hydrostatic thrust bearing is often affected by dynamic loads, so it is necessary to research the dynamic characteristics of hydrostatic thrust bearing. Geng [132] calculated damping and natural frequency of oil film of hydrostatic thrust bearing under different working conditions. Yu et al. [133] deduced the dynamic-static displacement ratio of oil film based on the dynamic equilibrium theory. The ratio ya/y of dynamic displacement to static displacement of oil film is as follows:

$$\frac{y_a}{y} = \frac{1}{\sqrt{\left[1 - \left(\frac{\omega_p}{\omega_0}\right)^2\right]^2 + \left(2\delta\frac{\omega_p}{\omega_0}\right)^2}} \tag{10}$$

where ω_0 is natural frequency of system, ω_p is sinusoidal loading frequency, δ is damp ratio. Curve of dynamic and static displacement ratio is shown in Fig. 25.

From the curve, it can be find that when sinusoidal load frequency is in the high frequency band, the dynamic displacement of oil film is small and oil film will not vibrate greatly, so the high frequency loading will not affect the stability of system, and the dynamic stiffness in the high frequency band is large and the amplitude is small, so system will not resonate. However, most of research on the dynamic characteristics of hydrostatic thrust bearing only take oil film as the specific research object, and the research on the whole hydrostatic thrust bearing is less. Therefore, the hydrostatic thrust bearing system should be selected as the research object in the future.

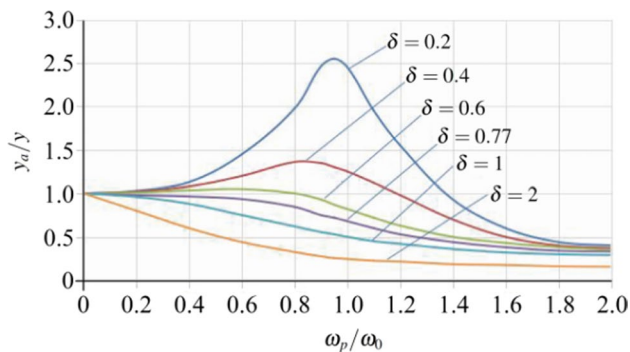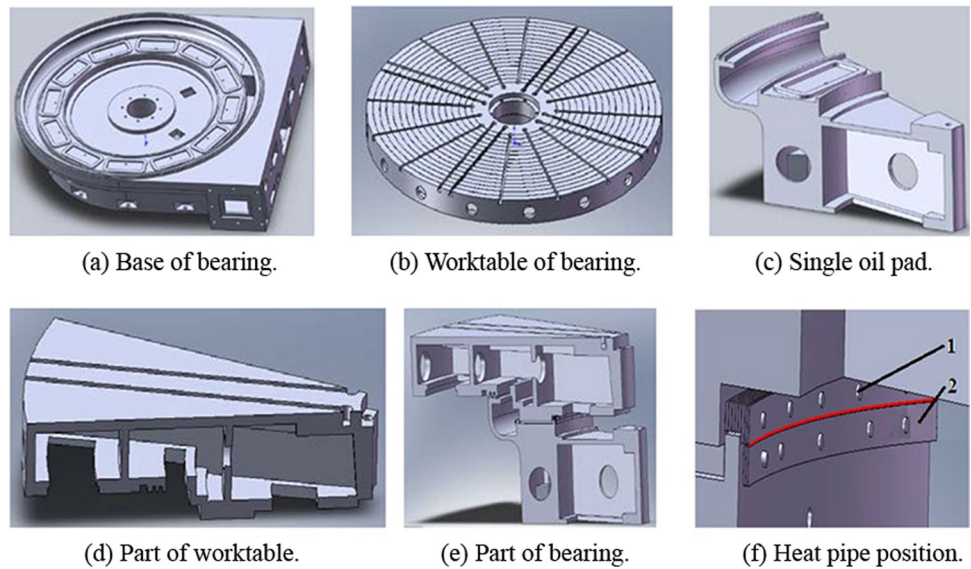**Fig. 24** Micro heat pipe structure of hydrostatic thrust bearing [131]

(a) Base of bearing.

(b) Worktable of bearing.

(c) Single oil pad.

(d) Part of worktable.

(e) Part of bearing.

(f) Heat pipe position.

Fig. 25 Curve of dynamic and static displacement ratio [133]

13 Research Progress of Hydrostatic-Hydrodynamic Thrust Bearing

Under extreme working condition of high speed and heavy load, temperature of hydrostatic bearing oil film increase, viscosity of hydrostatic bearing oil film decrease, and with extrusion and shearing of oil film, stiffness and bearing force of oil film decrease, it is easy to cause local boundary lubrication or dry friction [134]. To solve this problem, hydrodynamic bearing is added to hydrostatic bearing can improve oil film stiffness, and tribological failure is avoided, machining accuracy of machine tool is improved.

14 Research Progress of Hydrostatic-Hydrodynamic Thrust Bearing with Tilting Oil Pad

Brecher et al. [135] found that hydrostatic thrust bearing oil pad had dynamic pressure at oil return groove. Hydrostatic bearing gap between worktable and base is a parallel flat plate. In order to realize hydrostatic-hydrodynamic hybrid bearing effect, oil pad and base are connected together by pin. During rotation of worktable, oil pad can automatically tilt, thus hydrostatic- hydrodynamic hybrid bearing effect is formed [136, 137]. Hydrostatic-hydrodynamic hybrid bearing structure is shown in Fig. 26, tilting oil pad bearing structure is shown in Fig. 27.

In 1991, Osman et al. [138] studied inclination angle of hydrostatic thrust bearing oil pad. According to the tribological behavior of tilting hydrostatic thrust bearing with self-adaption oil pad, Sui [139] researched the influence of oil pad inclination angle and coupling inclination angle on the tribological characteristics of hydrostatic thrust bearing. Through simulation, it was found that when load was 10t and rotational speed was 140 r/min, inclination angle on the radial inner side of oil pad was 0.009°, and inclination angle on the downstream side was 0.005024°, self-adaptive inclination angle was 0.0088°, oil film bearing capacity was the largest and angle was the best. Wang [140] simulated oil film pressure field and temperature field under different oil pad inclination angles and different oil chamber areas, from the simulation results, it was found that the optimal oil pad inclination angle was 0.0044°, and the optimal oil chamber area percentage was 80%. Based on lubrication theory and tribology principle, Yu et al. [141] optimized structural parameters of tilting oil pad to adapt to the deformation of worktable and compensate
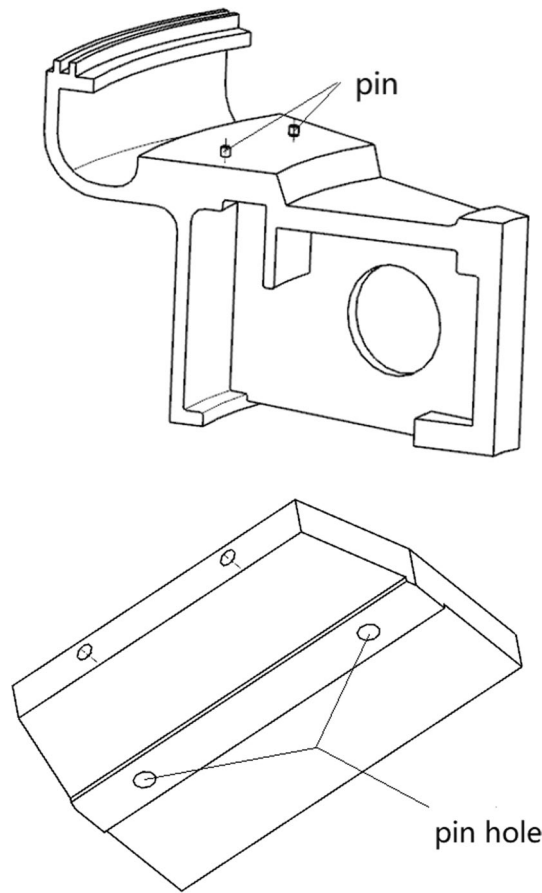
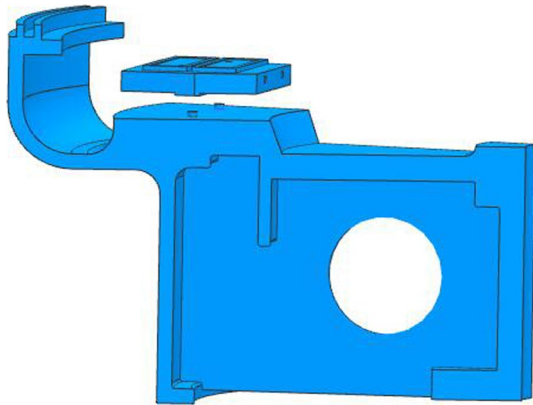**Fig. 26** Hydrostatic-hydrodynamic hybrid bearing structure

Fig. 27 Tilting oil pad bearing structure

Table 3 Optimum oil pad inclination angle values under different extreme conditions

Extreme working conditions	Circumferential inclination angle	Radial inclination angle
0t	0.0020°	0.0025°
4t	0.0035°	0.0040°
8t	0.0020°	0.0035°
12t	0.0025°	0.0045°
16t	0.0020°	0.0040°
20t	0.0015°	0.0040°
24t	0.0005°	0.0045°
28t	0.0010°	0.0045°
32t	0.0020°	0.0005°
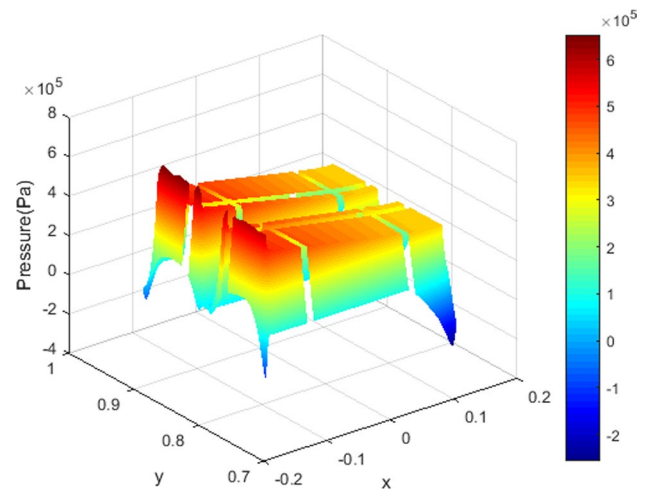
Fig. 28 Pressure field [142]

bearing with diameter of 3.5 m as research object, analyzed distribution of oil film pressure field, temperature field and flow field under different extreme working conditions, and determined optimal inclination angles of oil pad. The inclination angle values are shown in Table 3, pressure field of oil film is shown in Fig. 28 when load is 12t, oil pad inclination angle is 0.0015° and worktable rotational speed is 182.3 r/min, flow field are shown in Fig. 29 when circumferential inclination angle is 0.0015° and 0.0025°. From pressure field, it can be found that pressure on the downstream side of oil pad is larger. From Fig. 29, it can be found that when circumferential inclination angle is 0.0025°, oil particles have relatively few trajectories in the oil chamber, shearing times are less, temperature rise is lower and lubrication performance is better.

Yuan [143] simulated the deformation of friction pair of tilting oil pad hydrostatic thrust bearing, and visually expressed the shape of oil film through scatter diagram of MATLAB. Morphology of oil film is shown Fig. 30.

the lack of hydrostatic bearing. Through simulation and experiment, it was found that when the length and width of the bottom of tilting oil pad were 35 mm, the height was 1.5 mm, and clearance with 0.25 mm double pins was used to connection with the base, the hydrodynamic effect was the most obvious. Zuo [142] took hydrostatic thrust

(a) Circumferential inclination angle is 0.0015°

(b) Circumferential inclination angle is 0.0025°

Fig. 29 Flow field [142]

Fig. 30 Morphology of oil film under extreme conditions [143]

Qu [144] used Workbench to simulate deformation of hydrostatic-hydrodynamic thrust bearing, the results showed that when load was 0–28t, deformation of friction pair was mainly affected by thermal deformation, and the probability of dry friction was higher, when load was 28–32t, base was depressed inward under the influence of stress, it could offset squeezing effect of worktable

deformation on oil film, and the probability of dry friction was lower, so the load range of 28–32t was better under extreme working conditions. Yu et al. [145] used ANSYS Workbench to simulat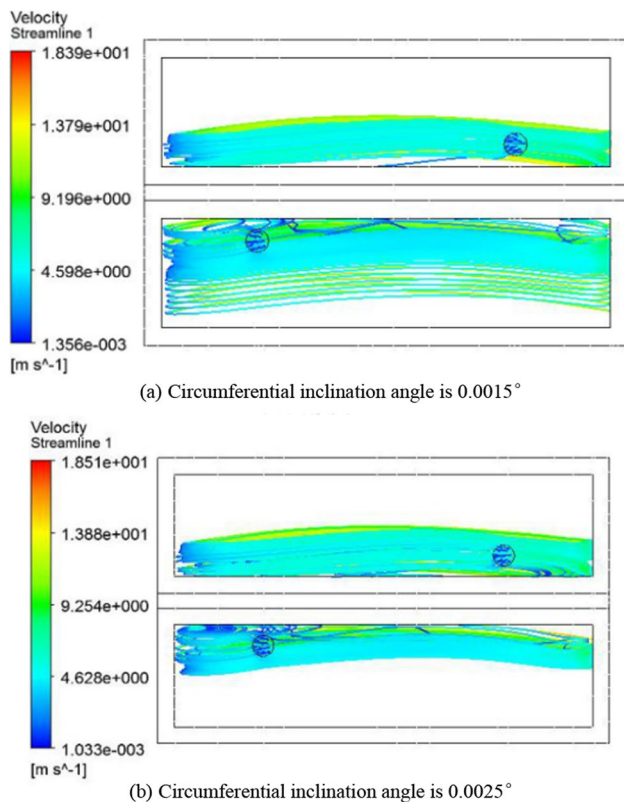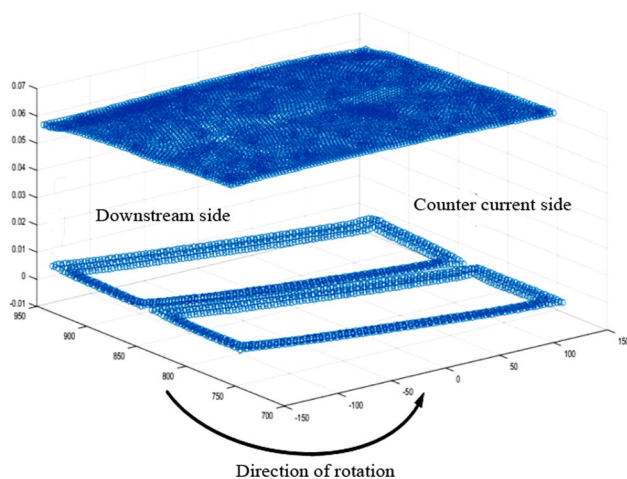e the deformation of oil pad tilting hydrostatic bearing friction pair, and obtained the thinnest oil film thickness under different loads and rotational speeds, which provided theoretical basis for the research on tribological failure mechanism. The thinnest oil film thickness under different working conditions is shown in Fig. 31. Zhou [146] used CFX to simulate oil film of hydrostatic-hydrodynamic thrust bearing, and found that pressure difference of hydrostatic-hydrodynamic thrust bearing was obviously larger than that of traditional hydrostatic thrust bearing, and hydrodynamic pressure effect of hydrostatic-hydrodynamic thrust bearing was more obvious.

In some research, the microstructure is added to surface of friction pair, which can form wedge-shaped gap, cause additional bearing capacity and achieve better hydrostatic-hydrodynamic hybrid bearing effect. Razzaque and Hossain [147] used the mathematical model based on narrow groove theory (NGT) to research the slotting effect in the porous hydrostatic circular stepped thrust bearing. The result showed that bearing capacity could be improved by slotting under the medium porous surface permeability. Wu [148] applied microstructure to hydrostatic thrust bearing, added rectangular grooves and triangular grooves on oil sealing edge and added strip grooves on oil chamber. Through simulation and experiment verification, it was found that the mixed microstructure could effectively increase bearing capacity under high load.
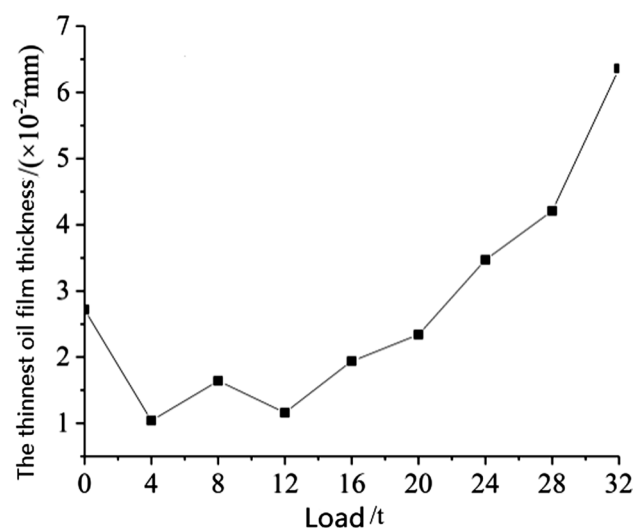

Fig. 31 The thinnest oil film thickness under different working conditions [145]
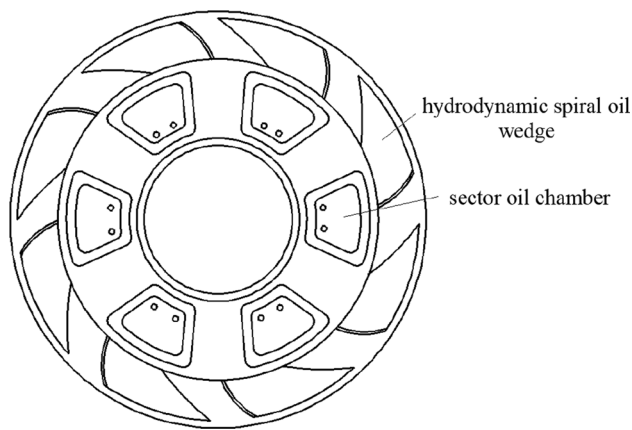
Fig. 32 Schematic diagram of oil chamber of hydrostatic-hydrodynamic hybrid rotary table [149]
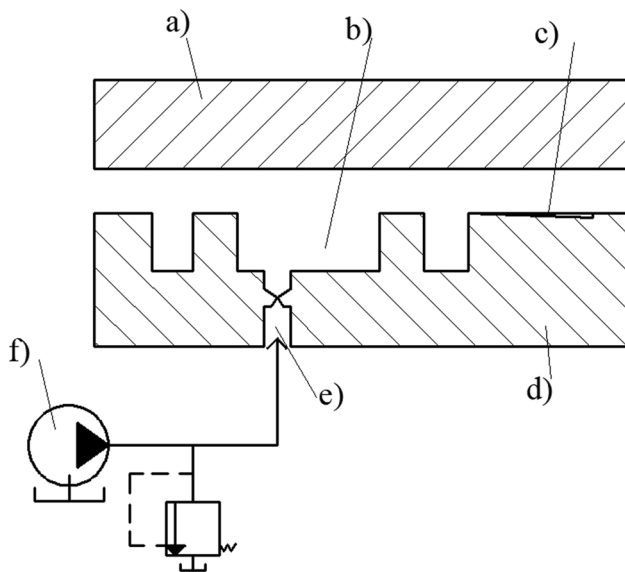

Fig. 33 Section view of oil chamber [150]. (a) Worktable, (b) oil chamber, (c) hydrodynamic spiral oil wedge, (d) Intermediate rotary table, (e) orifice throttler, (f) oil pump

15 Research Progress of Hydrostatic-Hydrodynamic Thrust Bearing with Spiral Oil Wedge

Ma et al. [149, 150] put a new type of hydrostatic-hydrodynamic rotary table structure, which had sector chamber and spiral oil wedge, thus hydrostatic-hydrodynamic hybrid bearing structure was realized. Schematic diagram and section view of oil chamber of hydrostatic-hydrodynamic hybrid rotary table are shown in Figs. 32 and 33. Liu et al. [151] established the mathematical model of bearing characteristics of hydrostatic-hydrodynamic hybrid rotary table by Reynolds equation and flow continuity equation,

Table 4 Optimal geometry parameters under different rotational speed

ω/(r/min)	β/°	h_1	$(h_0+h_1)/h_0$	n
10	28.27	380.52	3.72	12
20	28.36	380.45	3.72	12
30	28.29	380.23	3.72	12
40	28.11	380.41	3.72	12
50	28.24	380.74	3.72	12
60	28.36	380.58	3.72	12

Where ω is rotational speed, β is helix angle, h_1 is wedge depth, $(h_0+h_1)/h_0$ is film thickness ratio, n is wedge number

Table 5 Maximum rotational speeds under different oil film thicknesses

Oil supply pressure/ MPa	Maximum rotational speed/(r min^{-1})				
	0.04 mm	0.06 mm	0.08 mm	0.10 mm	0.15 mm
0.1	2.07	4.93	10.26	18.9	51.08
0.2	4.06	9.77	20.51	37.17	92.35
0.3	6.21	14.60	30.60	54.89	128.09

and found that flow rate of hydrostatic chamber was less than leakage of the hydrodynamic wedge under heavy load, and calculated the critical value of height difference between oil sealing surface of hydrostatic chamber and oil sealing surface of hydrodynamic wedge. When the height difference was greater than critical value, the problem of insufficient oil supply of hydrodynamic wedge could be solved. Nie et al. [152, 153] established a new mathematical model of oil film of hydrostatic-hydrodynamic rotary table to research the influence of rotational speed on bearing characteristics of oil film. It was found that with the increase of rotational speed, oil film thickness decreased, the bearing capacity of hydrodynamic area increased, stiffness and damping of oil film increased. Tian et al. [154] used cuckoo search to optimize geometry parameters of spiral oil wedge under different rotational speeds. The optimal structure parameters are shown in Table 4. In order to avoid the shortage of hydrodynamic oil wedge oil supply caused by negative pressure in the outer groove area of new type of hydrostatic-hydrodynamic rotary table chamber, Liu et al. [155, 156] obtained the maximum rotational speed without negative pressure in the outer groove area of oil chamber under different oil film thicknesses by Fluent, improved structure of hydrostatic oil chamber and hydrodynamic groove, the negative pressure phenomenon was avoided. Maximum rotational speeds under different oil film thickness are shown in Table 5.

The best combination scheme of hydrostatic-hydrodynamic is determined by selecting the best inclination angle

of oil pad. Hydrostatic-hydrodynamic thrust bearing is generally applied in rotary table, and it can also be applied in closed circular guideway with high rotational speed and heavy load. Instead of traditional rolling bearing, hydrostatic-hydrodynamic thrust bearing can improve lubrication performance and avoid tribological failure.

16 Research Progress of Hydrostatic-Hydrodynamic Spindle

As one of the most important structures of CNC machine equipment, spindle's rotation accuracy and radial bearing stiffness directly determine machining performance of CNC machine equipment. Due to excursion of the center of spindle, two friction pair surfaces form angle, which lead to additional hydrodynamic effect appear. Hydrostatic-hydrodynamic spindle can greatly improve rotation accuracy, bearing stiffness and vibration resistance [157, 158]. The radial bearing structure of hydrostatic-hydrodynamic spindle is shown in Fig. 34.

17 Research Progress of Lubrication Performance of Hydrostatic-Hydrodynamic Spindle

Phalle et al. [159–161] controlled flow and eccentricity by flow control device, improved the performance of hydrostatic-hydrodynamic bearing. Santos et al. [162, 163]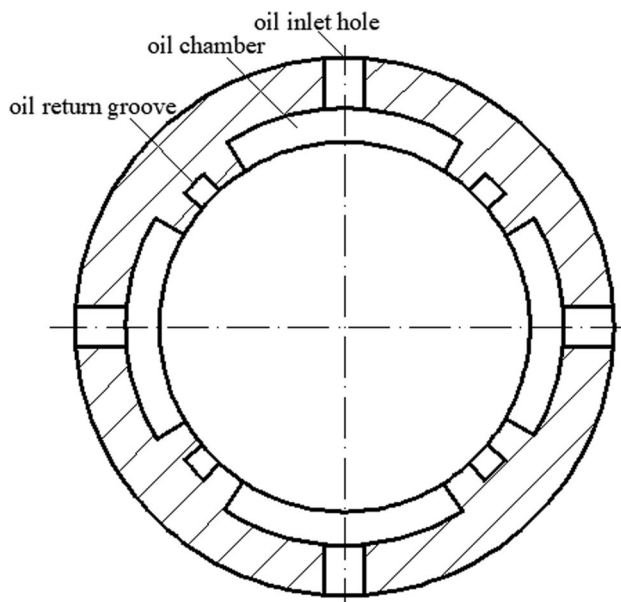 considered that active lubrication by active control method could improve damping coefficient, motion accuracy and stability of hydrostatic bearing. Based on hydrostatic bearing, controllable throttle can actively control pressure in oil chamber to maximize oil film stiffness under different working conditions, thus motion accuracy and stability of hydrostatic-hydrodynamic spindle are improved [164–166]. Singh et al. [167] changed flow rate and pressure of oil supply through controllable throttle, which improved stiffness of oil film of hydrostatic-hydrodynamic spindle. Hu et al. [168, 169] put a pre-controlled throttling technology, which could increase oil film stiffness by about 50%. Controllable throttle structure is shown in Fig. 35. Zhang [170] established mathematical models of different throttles, analyzed the influence of throttles type and throttle ratio on oil film stiffness of hydrostatic bearing, and found that oil film stiffness was the highest when throttle ratio of capillary throttle was about 2 and that of orifice throttle was about 1.71. Based on the differential effect of the piezoelectric thin film differential throttle valve, Liu et al. [171] connected two oil outlets of throttle valve with two opposing oil chambers, thus indirectly obtained the movement track of hydrostatic-hydrodynamic spindle axis. Xia et al. [172] simulated the bearing capacity of hydrostatic-hydrodynamic spindle oil film, the result showed that the bearing capacity of hydrostatic-hydrodynamic spindle was the largest when diameter of spindle orifice was 0.5 mm.

In the research on lubrication characteristics of hydrostatic-hydrodynamic spindle oil film. Wang et al. [173] simulated the temperature rise of oil film of hydrostatic-hydrodynamic spindle of ultra-high speed grinder by Fluent,

Fig. 34 Structure of radial bearing

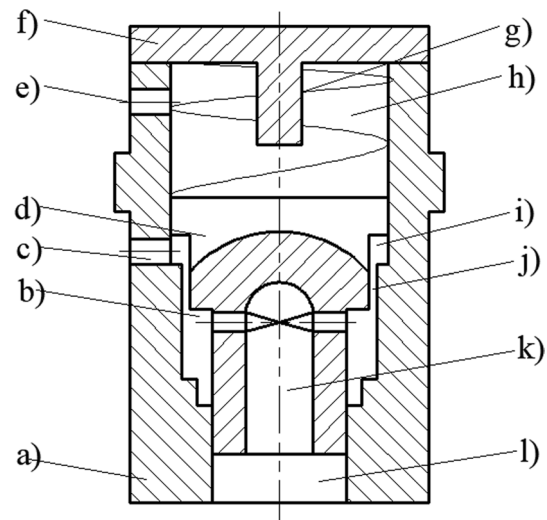**Fig. 35** The diagram of controllable throttle structure [169]. (a) Sleeve of throttler, (b) Integrated oil chamber, (c) Oil inlet hole of throttler, (d) Stepped throttle column, (e) Oil outlet hole of control oil chamber, (f) Cover of throttler, (g) Spring, (h) Control oil chamber, (i) Choke inlet oil chamber, (j) Annular throttle clearance, (k) Oil outlet hole of bearing oil chamber, (l) Bearing oil chamber

and found that the spindle rotational speed was the main influence factor of oil film temperature. Yu et al. [174] took hydrostatic-hydrodynamic spindle of ultra-high speed grinder as research object, calculated the stiffness of oil film at different spindle speeds through dynamic grid technology, and determined the critical speeds of spindle with and without prestressing force were 13,550 r/min and 14,700 r/min through modal analysis, it provided a theoretical reference for the resonance of hydrostatic-hydrodynamic spindle of ultra-high speed grinder was avoided. The stiffness of oil film in X direction and Y direction under different speeds are shown in Table 6.

Chen et al. [175] established mathematical models of bearing capacity, stiffness and dynamic stiffness of hydrostatic-hydrodynamic spindle with oil film slip, and found that oil film slip at micro scale could improve bearing capacity and stiffness of hydrostatic-hydrodynamic spindle. Pham et al. [176] researched the influence of oil supply pressure and lubricating oil viscosity on the stiffness of hydrostatic-hydrodynamic spindle of grinder. The results showed that with the increase of lubricating oil viscosity, the stiffness of hydrostatic-hydrodynamic spindle increased, with the increase of oil supply pressure, the stiffness of hydrostatic-hydrodynamic spindle increased when oil supply pressure of pump was 3–5 MPa.

18 Research Progress of Structure of Hydrostatic-Hydrodynamic Spindle

The geometric error of hydrostatic-hydrodynamic spindle has a large influence on its lubrication characteristics and motion accuracy. Abele et al. [177–179] researched the influence of eccentricity on stiffness and accuracy of spindle of high-speed precision and ultra-precision machine tools based on hydrostatic bearing, and predicted its rotation accuracy. Hou et al. [180] simulated the rotation error trajectory of hydrostatic-hydrodynamic spindle by dynamic grid technology, and found that the circular error of shaft journal had large influence on the rotation accuracy of spindle, and through experiment, it was found that the coincidence

Table 6 Stiffness of oil film under different spindle speeds

Rotational speed/(kr/min)	Kxx/(MN/m)	Kyy/(MN/m)
0	531	344
2	592	387
5	668	436
8	758	501
10	803	542
15	901	627
20	944	665

between theoretical calculation results and experimental test results was 75.2%. According to the error average effect model of hydrostatic sliding bearing, Zha et al. [181] found that the shape error of shaft had a large influence on the spindle rotation accuracy. Zhang and Chen [182] established the approximate error motion model of hydrostatic-hydrodynamic spindle, and analyzed the internal relationship between geometric error and motion error of spindle. The results showed that the circular error of shaft journal had larger influence on motion error than the proper alignment error of the shaft journal and the verticality error of front thrust plate. Fang et al. [183] established the linear model of rotor dynamics equation with five degrees of freedom to determine the motion track of hydrostatic-hydrodynamic spindle rotor, and found that spindle run-out was more sensitive to rotor proper alignment error and oil film gap through simulation.

On the improvement of hydrostatic-hydrodynamic spindle structure, Yamada et al. [184, 185] considered that the initial radial bearing stiffness could indirectly calculate the best gap size, which provided a theoretical basis for the modification of spindle gap size. Lin [186] simulated the temperature field of oil film of rectangular chamber and trapezoidal chamber by Fluent under different spindle rotational speeds, it was found that the temperature rise of rectangular chamber was larger than that of trapezoidal chamber under the same working condition. Based on TRIZ conflict theory, Zhang [187] improved oil chamber structure of hydrostatic bearing, and simulated oil film pressure field and temperature field under different spindle rotational speeds. The result showed that the performance of bearing with six oil chambers was better than that of bearing with four oil chambers. Zhang et al. [188] established Kriging surrogate model, optimized conical hydrostatic-hydrodynamic bearing structure to improve bearing capacity and reduce temperature rise.

Deep-shallow chamber structure is generally used to achieve the effect of hydrostatic-hydrodynamic hybrid bearing better. The structure of deep-shallow chamber hydrostatic and hydrodynamic hybrid bearing is shown in Fig. 36.

Guo et al. [189] used CFD to research the influence of structure parameters of deep-shallow chamber hydrostatic-hydrodynamic bearing on stiffness and temperature rise. The results showed that when the bearing design clearance was 0.03 mm and the oil inlet hole diameter was 0.7 mm, bearing stiffness was the highest and oil film temperature rise was the lowest, and shallow chamber depth of 0.06–0.08 mm could keep temperature rise of oil film low. Wang and Jiang [190] analyzed the hybrid bearing capacity characteristics under different chamber depths. The result showed that with the decrease of shallow groove depth, the bearing capacity increased. Based on the principle of flow balance, Meng et al. [191] established mathematical model of hydrostatic-hydrodynamic bearing with orifice throttle, and revealed
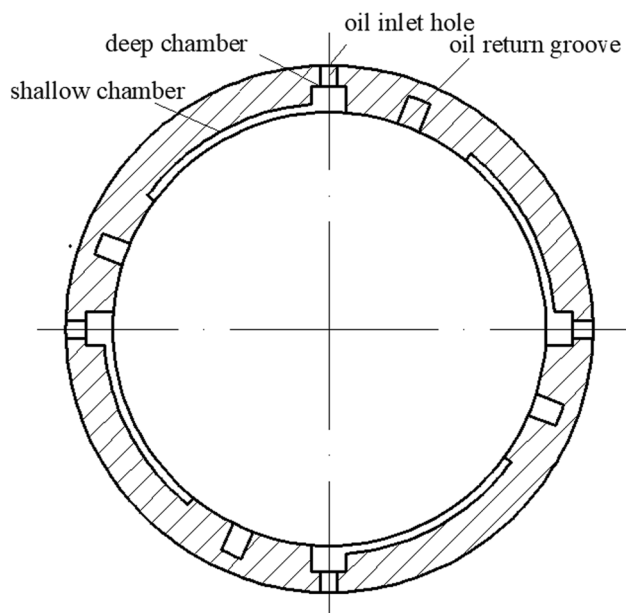
Fig. 36 Structure of deep-shallow chamber hydrostatic-hydrodynamic hybrid bearing

the influence law of shallow chamber depth and initial oil film thickness on the bearing performance of hydrostatic-hydrodynamic bearing. It was found that when shallow chamber depth was 2–3 times of initial oil film thickness, bearing stiffness was the highest and temperature rise was the lowest. Guo et al. [192] took hydrostatic- hydrodynamic spindle of high precision grinder as the research object, established fluid–structure interaction model of hydrostatic-hydrodynamic bearing, and found from static and dynamic that the changes of static deflection and dynamic deflection of spindle system were bigger than the spindle rotation accuracy under the influence of bearing oil film temperature rise, which showed that the bearing oil film temperature rise characteristics could obviously affect the accuracy of high-precision grinding spindle system. Wang et al. [193, 194] created oil film mesh of hydrostatic-hydrodynamic bearing by ICEM CFD, changed eccentricity of oil film by dynamic mesh method, and simulated pressure distribution and temperature distribution of oil film of deep-shallow chamber. The results showed that bearing capacity and temperature rise of oil film increased with the increase of eccentricity and rotational speed, and the influence of rotational speed on oil film temperature rise was greater than eccentricity. Zhang et al. [195] analyzed the variation law of bearing capacity and temperature rise of oil film under different oil film thickness and deep chamber angle by numerical simulation. The results showed that when oil film thickness was 0.03 mm, bearing capacity was the largest and temperature rise was the lowest, and when deep chamber angle was 10°, hydrodynamic effect of oil film was obvious. Liu [196] simulated

oil film bearing capacity of hydrostatic-hydrodynamic bearing by Fluent, and found that with the increase of oil inlet hole, bearing capacity and stiffness of oil film increased at first and then decreased under a certain eccentricity, determined optimal oil inlet hole diameter. Liu and Li [197] took hydrostatic-hydrodynamic bearing with four oil chambers as the research object, and obtained the influence of different oil inlet diameters on the maximum oil film pressure by Fluent. The results showed that with the increase of oil inlet diameter, the maximum oil film pressure increased, and when oil inlet diameter reached a certain value, the maximum oil film pressure was stable. Ding and Liu [198] took the minimum oil film temperature rise, the maximum oil film stiffness and bearing capacity as the object functions, optimized parameters of hydrostatic-hydrodynamic bearing, such as shallow chamber depth, initial oil film thickness and oil inlet diameter, and improved the working performance of ultra-high speed cutting spindle. Guo et al. [199] took power consumption, temperature rise and threshold rotational speed as optimization objectives, and optimized hydrostatic-hydrodynamic bearing by complex method. The results showed that when half cone angle, width of oil sealing edge and shallow chamber angle were reduced, power consumption and temperature rise were effectively reduced, and threshold rotational speed was increased. Wei et al. [200] established mathematical model of bearing capacity of hydrostatic-hydrodynamic bearings, and carried out experimental verification. It was found that stiffness increased with the increase of rotational speed, and stiffness value was stable when rotational speed was 3000–6000 r/min.

19 Research Progress of Fluid–Structure Interaction Deformation of Hydrostatic-Hydrodynamic Spindle

Fluid–structure interaction deformation can affect bearing stiffness and motion accuracy of hydrostatic-hydrodynamic spindle. Yuan [201] analyzed the thermal deformation of hydrostatic-hydrodynamic spindle with controllable throttle by fluid-heat-structure interaction model, and verified accuracy of theory through experiments. Though finite element analysis and numerical simulation, Nagasaka et al. [202] found that the local deformation of spindle would be caused under influence of fluid pressure, and the bearing stiffness would be reduced by about 10%. According to requirements of bearing performance of spindle of high-speed grinder, Zhao et al. [203] made fluid–structure interaction simulation of high precision hydrostatic-hydrodynamic spindle by Fluent and Workbench. From the simulation results, it was found that the temperature rise of spindle rotor played an important role in axial deformation and stress concentration of spindle. Kuznetsov and Glavatskih [204] analyzed

the thermal deformation of hydrostatic bearing, and found that the thermal deformation had a great influence on stiffness and damping of bearing. According to the influence of hydrostatic-hydrodynamic spindle deformation on oil film gap, Zhang [205] established mathematical models of fluid control equation, and combined simulation and experiment found that force deformation could compensate thermal deformation, spindle rotational speed and viscosity-temperature effect had large influence on the deformation of bearing shell, spindle and oil film. Tang et al. [206] established the thermal-fluid–structure interaction model of hydrostatic bearing, and found that the maximum thermal deformation of bearing shell along the X axis was about 18.2 µm, the Y axis was about 12.1 µm, the thermal deformation of bearing could reduce the spindle rotation accuracy. Yin et al. [207, 208] established the thermal-fluid–structure interaction model of hydrostatic-hydrodynamic spindle of ultra-precision horizontal machine tool, simulated temperature rise and deformation of spindle system under different working conditions, and through experimental verification, it was found that the error between experiment results and simulation results was 2.5%. At the same time, parameters of bearing outside diameter, bearing placement, spindle diameter and spindle length of hydrostatic-hydrodynamic spindle system were optimized to reduce the temperature rise and improve the bearing stiffness of hydrostatic-hydrodynamic spindle system. Yang [209] entered UDF program, simulated pressure field and temperature field of oil film with variable viscosity by Fluent, and simulated the deformation of radial bearing by fluid–structure interaction. The result showed that the maximum deformation of bearing appeared at the axial edge. Du [210] put an adjustable oil film gap hydrostatic bearing, which could make oil film reach a specific thickness to improve spindle rotation accuracy by adjusting inner cone steel sleeve and left and right covers. Chen et al. [211] carried out fluid–structure interaction simulation and experimental verification on hydrostatic-hydrodynamic spindle, and found that spindle system had micro-scale effect and slip phenomenon in actual operation, and the error between experiment and simulation was within 10%.

From the research progress of hydrostatic-hydrodynamic spindle, it can be found that fluid–structure interaction deformation and spindle geometric error all have different effects on the lubrication performance of hydrostatic-hydrodynamic spindle, the motion error of hydrostatic-hydrodynamic spindle can be compensated by changing oil supply flow rate, oil supply pressure and oil chamber structure. For hydrostatic-hydrodynamic spindle in high-speed operation, shear force may cause hot oil in a oil chamber to be carried into adjacent oil chamber, which will increase oil film temperature. Therefore, the influence of hot oil carrying factors on the thermal deformation of hydrostatic-hydrodynamic spindle should be considered.

The lubrication performance is improved of hydrostatic-hydrodynamic spindle by adjusting angle of deep chamber and shallow chamber, chamber depth and diameter of oil inlet hole in most of research. However, the tilting pad bearing structure can also achieve the effect of hydrostatic-hydrodynamic hybrid bearing, so it can be considered whether the tilting pad bearing structure can be combined with the deep-shallow chamber structure to improve the lubrication performance of radial bearing.

20 Conclusion

This paper reviewed the research progress of hydrostatic linear guideway, hydrostatic rest and ram, hydrostatic thrust bearing and hydrostatic-hydrodynamic spindle of high-end CNC machine equipment. In the research on dynamic characteristics of hydrostatic guideway, the hydrostatic bearing system can be regarded as a system with mass, spring and damper, which simplifies the dynamic model of hydrostatic guideway. Motion accuracy and stability of hydrostatic linear guideway can be improved by changing flow control valve and guideway structure. In the research on hydrostatic rest and ram of vertical lathe and milling machining center, oil film pressure, ram deformation and compensation are summarized, but the theoretical calculation of oil film pressure in each oil chamber of rest is simple. In the research on hydrostatic thrust bearing, the influence of working parameters, lubricating oil viscosity, oil chamber structure and friction pair deformation on the lubrication performance of hydrostatic thrust bearing is analyzed. In the research on dynamic characteristics of hydrostatic thrust bearing, the main research object is damping and natural frequency of oil film, but the research on the dynamic characteristics of whole hydrostatic thrust bearing is less. Under the condition of high speed and heavy load, centrifugal force and friction heat can lead to the decrease of oil film stiffness, and dry friction is caused. Therefore, hydrostatic-hydrodynamic hybrid bearing is suggested to make up for the lack of oil film stiffness, and avoid tribological failure. In order to realize the effect of hydrostatic-hydrodynamic hybrid bearing, the structure of hydrostatic thrust bearing with tilting oil pad and the structure of rotary table with hydrostatic oil chamber and spiral oil wedge are suggested. In the research on hydrostatic-hydrodynamic spindle, the active lubrication of hydrostatic-hydrodynamic spindle system is realized by controllable throttle. The influence of fluid–structure interaction deformation and geometric error on the bearing performance of hydrostatic-hydrodynamic spindle is analyzed, but the influence of hot oil carrying on the thermal deformation of hydrostatic-hydrodynamic spindle is also a key factor. In order to achieve the

effect of hydrostatic-hydrodynamic hybrid bearing better, deep-shallow chamber structure is suggested, the main research parameters are angle of deep chamber-shallow chamber, chamber depth and diameter of oil inlet hole.

21 Future

Some of great challenges will be the update of research method and direction on hydrostatic bearing and hydrostatic-hydrodynamic hybrid bearing. In the research method, the structure of hydrostatic linear guideway can be modified in advance by modification method to realize deformation compensation according to the deformation law. The theoretical calculation method of oil film pressure of hydrostatic rest and ram is simple. Oil film pressure and stiffness can be indirectly calculated by elastic model replace oil film in simulation, or directly obtained by pressure sensor in experiment. In the aspect of structure optimization of hydrostatic bearing and hydrostatic-hydrodynamic hybrid bearing, the optimal structure can be obtained by Neural network algorithm, such as shape and size of oil chamber, size and position of microstructure.

In the research direction, modal analysis can be carried out on whole hydrostatic thrust bearing under different dynamic parameters of oil film, and the influence of damping, natural frequency and dynamic stiffness of oil film on dynamic characteristics of hydrostatic thrust bearing system can be analyzed. The application field of hydrostatic-hydrodynamic thrust bearing also needs to be expanded. Besides being applied to rotary table of CNC machine equipment, hydrostatic-hydrodynamic thrust bearing can also be applied in closed circular guideway with high speed and heavy load, and replaces traditional rolling bearing. It may open up a new way for application and research of hydrostatic-hydrodynamic hybrid bearing. In the research on thermal deformation of hydrostatic-hydrodynamic spindle, the influence factor of hot oil carrying should also be considered. Besides deep-shallow chamber structure, tilting pad hydrostatic-hydrodynamic bearing structure is suggested in some research. Chen et al. [212, 213] put a single tilting pad hydrostatic bearing, which realized the common bearing of tilting pad hydrodynamic force and oil chamber hydrostatic. In the future research, tilting pad structure and deep-shallow chamber structure can be combined to analyze whether the lubrication performance of hydrostatic-hydrodynamic spindle can be improved.

References

1. Charki, A., Diop, K., Champmartin, S., & Ambari, A. (2013). Reliability of a hydrostatic bearing. *Journal of Tribology, 136*(1), 249–256.
2. Manring, N. D., Johnson, R. E., & Cherukuri, H. P. (2002). The impact of linear deformations on stationary hydrostatic thrust bearings. *Journal of Tribology, 124*(4), 874–877.
3. Zha, J., Xue, F., & Chen, Y. (2017). Straightness error modeling and compensation for gantry type open hydrostatic guideways in grinding machine. *International Journal of Machine Tools and Manufacture, 112*, 1–6.
4. Ding, Z. Q. (1986). *Hydrostatic bearing design*. Shanghai Scientific & Technical Publishers.
5. Yu, X. D. (2019). *Lubrication technology of thrust bearing under high speed and heavy load*. Science Press.
6. Pang, Z. C. (1982). A theoretical research on the dynamic stability of hydrostatic bearing. *Journal of Harbin Institute of Technology, 3*, 86–98.
7. Shun, Z. L., Yan, Y. T., & Tian, W. L. (2015). *Mechanical design* (2nd ed.). Science Press.
8. Dong, W., Li, B., Guo, W., & Zhou, Q. (2019). Deformation analysis of hydrostatic guideways based on the cantilever plate bending calculation method. *Tribology Transactions, 62*(6), 1142–1154.
9. Zhu, J. B., & Jiang, S. Y. (2020). Stiffness modelling of cylindrical hydrostatic guideways. *Journal of Physics: Conference Series, 1650*(22), 22–26.
10. Xue, F., & Zhao, W. H. (2010). Influencing factors on error averaging effect of hydrostatic guideway. *Journal of Xi'an Jiaotong University, 44*(11), 33–36.
11. Li, W. F., Du, Y. T., & Li, M. (2012). The performance simulation study of the hydrostatic guideway of precision CNC lathe. *Machine Tool & Hydraulics, 40*(5), 14–17.
12. Li, S., Song, J. C., Wang, C. Z., Ren, G.A. (2014). Structural design and research on oil chamber flow field for closed hydrostatic guideway of precision CNC machine. *Machine Tool & Hydraulics, 42*(15), 85–87.
13. Bouzidane, A., & Thomas, M. (2007). Equivalent stiffness and damping investigation of a hydrostatic journal bearing. *Tribology Transactions, 50*, 257–267.
14. Bouzidane, A., Thomas, M., & Lakis, A. A. (2008). Nonlinear dynamic behavior of a rigid rotor supported by hydrostatic squeeze film dampers. *Journal of Tribology, 130*(4), 041102.
15. Bouzidane, A., & Thomas, M. (2013). Nonlinear dynamic analysis of a rigid rotor supported by a three-pad hydrostatic squeeze film dampers. *Tribology Transactions, 56*, 717–727.
16. Zhang, F. J. (2015). *Research on design and key technology of the hydrostatic guide way experiment platform*. Donghua University.
17. Zhang, L. (2011). *Study on the self-adaptive oil supply system of constant pressure of opened hydrostatic slider*. Donghua University.
18. Das, N. C. (1999). A study of optimum load capacity of slider bearings lubricated with power law fluids. *Tribology International, 32*, 435–441.
19. Wang, Z. W., Liu, Y., & Wang, F. (2017). Rapid calculation method for estimating static and dynamic performances of closed hydrostatic guideways. *Industrial Lubrication and Tribology, 69*(6), 1040–1048.
20. Liu, Y. L. (2010). *Analysis of static and dynamic characteristics of ultra-precision hydrostatic guideway and identification of model parameters*. Harbin Institute of Technology.
21. Liu, J. Y. (2020). *Research on static and dynamic characteristics of hydrostatic guide rail*. Xi'an University of Technology.

22. Wu, P. F., Gao, F., & Li, Y. (2020). Hydrostatic guide parameter identification in junction space based on frequency response function. *Machine Tool & Hydraulics, 48*(16), 5–9.

23. Zhao, J. H., Gao, D. R., & Zhang, Z. C. (2012). Indeterminate mechanics model of bearing capacity of constant pressure oil pockets in hydrostatic slide. *Journal of Mechanical Engineering, 48*(22), 168–176.

24. Zhao, J. H., & Gao, D. R. (2013). Influence of oil film thickness on characteristics of closed type hydrostatic slide. *China Mechanical Engineering, 24*(11), 1421–1430.

25. Zhao, J. H., & Gao, D. R. (2013). Dynamic characteristics analysis of liquid hydrostatic slide based on flow control valve. *China Mechanical Engineering, 24*(4), 444–451.

26. Gao, D. R., Wei, Y., & Wang, K. (2014). Influence of design parameters of cylindrical hydrostatic slide on its' performance. *Journal of Mechanical Engineering, 50*(24), 186–190.

27. Wang, Z. W., Zha, J., Chen, Y. L., & Zhao, W. H. (2014). Influencing of fluid-structure interactions on static and dynamic characteristics of oil hydrostatic guideways. *Journal of Mechanical Engineering, 50*(9), 148–152.

28. Lai, Z., Qiao, Z., Zhang, P., Wang, B., & Wu, Y. (2016). The effect of structural coefficient on stiffness and deformation of hydrostatic guideway. In *International symposium on advanced optical manufacturing and testing technologies* (p. 9685).

29. Zhang, Z. C. (2012). *Theoretical and simulation analysis of static and dynamic characteristics of hydrostatic guideway with PM controller*. Yanshan University.

30. Shi, C., Wang, Z., Peng, Y., Li, C., & Kong, L. (2020). Influence of PM controller parameters on motion accuracy of hydrostatic guideways. *Journal of Mechanical Engineering, 56*(1), 157–165.

31. Du, X., He, Y. Q., & Xin, X. W. (2021). Application of close-type hydrostatic guide in precision surface grinding machine. Precise. *Manufacturing & Automation, 2*, 62–64.

32. Zhang, X. Y. (2011). Amended calculation and application of hydrostatic system of constant current closed hydrostatic guideway. *Machine Tool & Hydraulics, 39*(19), 56–58.

33. Guo, A., Li, M. Y., Wang, F. L., Ma, X. (2020). Analysis of the support characteristics of the oil film of ultra-precision hydrostatic guideway. *Modular Machine Tool & Automatic Manufacturing Technique, 9*, 57–66.

34. Gao, D. R., Zhao, J. H., & Zhang, Z. C. (2013). Analysis of number of oil-pockets in one slid surface of liquid hydrostatic slide. *Engineering Mechanics, 30*(4), 423–428.

35. Liu, Q. (2016). *Research on flow simulation and mechanical properties of hydrostatic guide-way*. Xi'an University of Technology.

36. Wang, Y. L. (2020). *Research on motion linearity model and regulation technology of closed hydrostatic guide*. Xi'an University of Technology.

37. Chen, G. L., Yang, H., Liu, Y. H., Yin, C.Z., Jiang, Z., Li, Z.X. (2020). Series composite throttling closed hydrostatic guideway. Sichuan Province: CN112548595A, 2021-08-10.

38. Li, X. Z., Qiu, Y. F., Su, X., Wei, W., Li, J.S., Yang, H. (2020). Hydrostatic guideway system with active controllable oil film thickness. Sichuan Province: CN112077616B, 2021-08-10.

39. Ma, H., & Ran, C. C. (2021). Optimal design of hydrostatic guide rail based on Taguchi method and genetic algorithm. *Machine Tool & Hydraulics, 49*(2), 93–98.

40. Liu, X., Chen, Y., Zha, J., & Zhang, P. (2021). Research on improved hydrostatic guideway base thermal characteristics by flattening temperature distribution. *International Journal of Advanced Manufacturing Technology, 15*(5), 1735–1744.

41. Chen, Y. Q., Wu, Y. J., Zeng, W. P., Liu, Y.L., Gao, Y.Y., Gao, P., Zhou, W., Wang, L.Y., Guo, L. (2021). Sliding assembly of ultra-precision hydrostatic guideway. Hunan Province: CN112901659A, 2022-04-01.

42. Chen, Z., Zheng, L. G., Liu, H. L. (2021). Oil film hydrostatic guideway device. Jiangsu Province: CN213795225U, 2021-07-27.

43. Wu, F. X., Xu, Y. L., Deng, J. H., Deng, G.Y. (2021). Anti-torsion hydrostatic guideway of CNC machine tool. Beijing: CN113001198A, 2021-06-22.

44. Cha, J., Li, C. (2021). Method and system for evaluating motion accuracy of four-oil pad hydrostatic guideway. Jiangsu Province: CN113108750A, 2021-07-13.

45. Xiang, J. W., Wang, R., & Xu, J. Y. (2009). Structural finite element analysis of spindle ram for large-scale milling planer. *Manufacturing Technology & Machine Tool, 9*, 47–49.

46. Yang, M. Y., Xu, K. P., Wang, J. H., Peng, L.F. (2011). Research on deformation compensation for square ram of TK6926 CNC floor type boring & milling machine based on FEM technology. *Machine Tool & Hydraulics, 39*(4), 39–42.

47. Qiu, Z. X., Gao, Z. L., Ren, D., Cui, D.Y. (2020). Finite element analysis and optimization design for ram of bridge gantry milling machine. *Machinery Design & Manufacture, 9*, 162–166.

48. Lu, J., Wei, D. Q., Wang, R., Feng, J.G. (2016). Research on deformation law for the ram based on thermal-structural coupling. *Modular Machine Tool & Automatic Manufacturing Technique, 9*, 20–23.

49. Li, B. B., Liu, X., Li, S. P., Peng, L.F. (2017). Ram comprehensive thermal compensation study. *Machine Tool & Hydraulics, 45*(13), 68–72.

50. Rahman, M., Heikkala, J., & Lappalainen, K. (2000). Modeling measurement and error compensation of multi-axis machine tools. *International Journal of Machine Tools and Manufacture, 40*(10), 1535–1546.

51. Gu, D. Q., Zheng, Y. T., & Gu, W. H. (2015). Theoretical analysis and experiment of ram gap compensation's characteristics. *China Mechanical Engineering, 26*(3), 293–298.

52. Gao, Z. L., Qiu, Z. X., Ren, D., Cui, D.Y. (2019). Multi-objective preference design for ram of gantry milling machine based on orthogonal experimental method. *Modern Manufacturing Engineering, 5*, 97–103.

53. Liu, W. Z. (2008). Finite element analysis and deformation compensation technology of NC horizontal milling machine. *Modern Manufacturing Engineering, 30*(1), 56–58.

54. Wu, F. H., & Zhao, F. B. (2012). A compensation method for deflection of ram with combined pull and push rods. *China Mechanical Engineering, 23*(22), 2667–2670.

55. Yu, J. W., Gui, L., Li, X. M., & Zhang, H. (2015). FEM analysis and compensation of the ram deformation of CNC floor type boring milling machine tool. *Journal of Hunan University (Natural Sciences), 42*(10), 43–47.

56. Yu, X. D., Gao, W. C., Wu, G. P., Zhou, W., Bi, H., Wang, Y., Wang, J., & Jiao, J. (2021). Research status of hydrostatic bearing technology in machine tool. *Recent Patents on Mechanical Engineering, 14*, 1–9.

57. Yang, J. M. (2014). *The constructural research and design of ram in the heavy-duty vertical lathe*. Yanshan University.

58. Cheng, H. K. (2018). *Study on the lubrication performance of the vertical slide guide of the hydrostatic pillow*. Harbin University of Science and Technology.

59. Wang, Y. M., Liu, Z. F., Cai, L. G., & Cheng, Q. (2018). Modeling and optimization of nonlinear support stiffness of hydrostatic ram under the impact of cutting force. *Industrial Lubrication and Tribology, 70*(2), 316–324.

60. Wang, Y. M., Liu, Z. F., Cheng, Q., Zhao, Y., Wang, Y., & Cai, L. (2019). Analysis and optimization of nonlinear carrying performance of hydrostatic ram based on finite difference method and Runge–Kutta method. *Advances in Mechanical Engineering, 11*(6), 1–12.

61. Zhang, Y. Q., Hou, J. J., Gao, W. C., Zhao, Z. W., Zhou, D. F., & Cheng, H. K. (2020). Prediction model of the clearance oil film for static vertical rail considering the ram deformation. *Proceedings of the Institution of Mechanical, 234*(1), 42–49.

62. Gao, W. C. (2021). *Research on bearing performance of hydrostatic ram of vertical lathe under high speed and heavy load conditions*. Harbin University of Science and Technology.

63. Zhou, Z. D. (2013). *Research on spindle ram components error compensation of floor milling-boring machining center*. Soochow University.

64. Wu, F. H., Qiao, L. J., & Xu, Y. L. (2012). Deformation compensation of ram components of super-heavy-duty CNC floor type boring and milling machine. *Chinese Journal of Aeronautics, 25*, 269–275.

65. Zheng, Y. T. (2013). *Research on hydraulic compensating system for ram's slide guide of NC machine*. Zhejiang University.

66. Hua, X. L., Guo, X. H., & Pan, X. B. (2014). Analysis and research of ram hydrostatic guideway for large NC floor type boring and milling machine. *Machine Tool & Hydraulics, 42*(11), 59–61.

67. Hua, X. L. (2014). *The analysis and optimization of ram of large floor boring and milling machine*. Soochow University.

68. Gao, L. (2014). *The key technologies of GTM500200 lathing and milling center ram design*. Dalian University of Technology.

69. Wang, C. R., & Chen, Z. L. (2017). Experimental research on ram hydrostatic guideway of TH6918 machining center. *Coal Mine Machinery, 38*(11), 34–36.

70. Dong, T. J. (2017). *CNC floor type boring and milling machine analysis of ram's deformation and its compensation design*. Shanghai Jiao Tong University.

71. Yu, P., Jin, H., & Tong, K. (2017). Design and manufacturing of hydrostatic rolling combination guideway of vertical turning and milling center. *Machine Tool & Hydraulics, 45*(16), 11–13.

72. Ding, Z. Q. (2014). Development history and present situation of hydrostatic, hydrostatic and hydrodynamic technology in machine tools in China. *World Manufacturing Engineering & Market, 2*, 73–76.

73. Chen, B. X. (1991). *Fluid lubrication theory and its application*. The Machinery Publishing.

74. Chen, Y. S. (1980). *Principle and design of hydrostatic bearing*. National Defense Industry Press.

75. Pang, Z. C. (1981). *Hydrostatic and aerostatic technology*. Heilongjiang People's Publishing House.

76. Li, L. Q., Ma, L., & Wang, M. (2014). Heavy loading and high speed table design. *Manufacturing Technology & Machine Tool, 5*, 122–124.

77. Tian, Z. X. (2018). *Research on the characteristics and their affecting factors of the hydrostatic thrust bearing*. Huazhong University of Science and Technology.

78. Yu, X. D., Meng, X. L., Li, H. H., Tan, L., Wang, Z., Zhou, Q., Zhuang, J., & Yang, L. (2013). Pressure field of multi-pad annular recess hydrostatic thrust bearing. *Journal of Donghua University, 30*(3), 254–257.

79. Singh, U. P., Gupta, R. S., & Kapur, V. K. (2011). On the steady performance of hydrostatic thrust bearing: Rabinowitsch fluid model. *Tribology Transactions, 54*, 723–729.

80. Singh, U. P., Gupta, R. S., & Kapur, V. K. (2013). On the application of Rabinowitsch fluid model on an annular ring hydrostatic thrust bearing. *Tribology International, 58*, 65–70.

81. Tian, Z. X., Cao, H. Y., & Huang, Y. (2019). Static characteristics of hydrostatic thrust bearing considering the inertia effect on the region of supply hole. *Proceedings of the Institution of Mechanical Engineers Part J: Journal of Engineering Tribology, 233*(1), 188–193.

82. Yu, X. D., Qiu, Z. X., Li, H. H., & Tan, L. (2013). Lubrication performance and velocity characteristics of a multi-oil-pad hydrostatic thrust bearing with a sector-shaped cavity. *Journal of Engineering for Thermal Energy and Power, 28*(3), 296–300.

83. Wang, S. L., Xiong, W. L., Meng, S. G., Gui, L., Xue, J.Y. (2015). Analytical calculation and experimental research on the bearing capacity of fan-shaped hydrostatic thrust bearing supplied with constant oil flow. *Journal of Mechanical Strength, 37*(5), 828–832.

84. Yu, X. D., Sun, D. D., Wu, X. G., Sui, J. L., Liu, D., & Fu, X. (2016). High speed and heavy load characteristic on oil film thickness of annular recess multi-pad hydrostatic thrust bearing. *Journal of Propulsion Technology, 37*(7), 1350–1355.

85. Zhang, Y. Q., Quan, Z., Feng, Y. N., Kong, P.R., Sun, J.C. (2018). Dynamic analysis of internal flow field of double-rectangular cavity hydrostatic thrust bearing. *Journal of Mechanical Transmission, 42*(12), 109–113.

86. Rehman, W. U., Khan, W., Ullah, N., Chowdhury, M. S., Techato, K., & Haneef, M. (2021). Nonlinear control of hydrostatic thrust bearing using multivariable optimization. *Mathematics, 9*(8), 1–16.

87. Liu, G. D., Shao, J. P., Li, T. Y., Lin, Y.L., Hu, Y.X. (2021). Lubrication performance comparison of hydrostatic thrust bearing with different offset distances. *Journal of Harbin University of Science and Technology, 26*(3), 32–37.

88. Yu, X. D., Li, T., Meng, X. L., Li, H. H., Wang, Z. Q., Zhou, Q. H., & Yang, C. Q. (2013). Influence of rotational speed on oil film temperature of multi-sector recess hydrostatic thrust bearing. *Journal of the Chinese Society of Mechanical Engineers, 34*(5), 371–378.

89. Srinivasan, V. (2013). Analysis of static and dynamic load on hydrostatic bearing with variable viscosity and pressure. *Indian Journal of Science and Technology, 6*, 4777–4782.

90. Yu, X. D., Pan, Z., He, Y., Liu, S.H., Wei, Y.X. (2015). Simulation on flow patterns of gap oil film in heavy Type hydrostatic thrust bearing. *Journal of Harbin University of Science and Technology, 20*(6), 42–46.

91. Zhang, Y. Q., Feng, Y. N., Kong, P. R., Yu, X. D., & Kong, X. B. (2019). Temperature field and experiment of hydrostatic bearing oil film based on hot oil carrying. *Journal of Jilin University (Engineering and Technology Edition), 49*(4), 1203–1211.

92. Zhang, Y. Q., Feng, Y. N., Luo, Y., Yu, X.D. (2022). Hot oil carrying and oil film temperature rise characteristics of hydrostatic thrust bearings under various operating conditions. *Journal of Propulsion Technology*, 43(5), 1–9.

93. Singh, U. P., Gupta, R. S., & Kapur, V. K. (2012). On the steady performance of annular hydrostatic thrust bearing: Rabinowitsch fluid model. *Journal of Tribology, 134*, 044502.

94. Zhang, Y. Q., Fan, L. G., Li, R., Dai, C. X., & Yu, X. D. (2013). Simulation and experimental analysis of supporting characteristics of multiple oil pad hydrostatic bearing disk. *Journal of Hydrodynamics, 25*(2), 236–241.

95. Chen, Y. (2015). *Research on influence of lubrication oil physical property on performance of hydrostatic supporting oil-film*. Harbin University of Science and Technology.

96. Zhang, Y. Q., Zhang, Z.Q., Feng, Y. N., Kong, P. R., Sun, J.C., Kong, X.B. (2018). Lubrication characteristics of double rectangular cavity hydrostatic bearing at high speed. *Tribology, 38*(5), 609–618.

97. Zhang, Y. Q., Ni, S. Q., Zhang, Z. Q., Kong, P. R., Feng, Y. N., & Kong, X. B. (2019). Dynamic lubrication characteristics of oil film with variable viscosity hydrostatic sliding bearings at high speed. *Journal of Mechanical Engineering, 55*(22), 108–117.

98. Yu, X. D., Geng, L., Zheng, X. J., Wang, Z.X., Zhang, Y.Q. (2017). Oil film stiffness characteristics of constant fluid hydrostatic thrust bearing with annular cavity multi-pads. *Journal of Harbin Engineering University, 38*(12), 1951–19563.

99. Shen, F., Chen, C. L., & Liu, Z. M. (2014). Effect of pocket geometry on the performance of a circular thrust pad hydrostatic bearing in machine tools. *Tribology Transactions, 57*, 700–714.

100. Kumar, V., & Sharma, S. C. (2017). Combined influence of couple stress lubricant, recess geometry and method of compensation on the performance of hydrostatic circular thrust pad bearing. *Proceedings of the Institution of Mechanical Engineers, 231*(6), 716–733.

101. Chow, C. Y. (1975). A non-central feeding hydrostatic thrust bearing. *Journal of Fluid Mechanics, 72*(1), 113–120.

102. Sharma, S. C., Jain, S. C., & Bharuka, D. K. (2002). Influence of recess shape on the performance of a capillary compensated circular thrust pad hydrostatic bearing. *Tribology International, 35*(6), 347–356.

103. Heinrichson, N., Santos, I. F., & Fuerst, A. (2007). The influence of injection pockets on the performance of tilting-pad thrust bearings-part I: Theory. *Journal of Tribology, 129*(4), 895–903.

104. Heinrichson, N., Fuerst, A., & Santos, I. F. (2007). The influence of injection pockets on the performance of tilting-pad thrust bearings-part II: Comparison between theory and experiment. *Journal of Tribology, 129*(4), 904–914.

105. Yadav, S. K., & Sharma, S. C. (2016). Performance of hydrostatic textured thrust bearing with supply holes operating with non-Newtonian lubricant. *Tribology Transactions, 59*(3), 408–420.

106. Yadav, S. K., & Sharma, S. C. (2016). Finite element analysis of tilted thrust pad bearings of various recesses shapes considering thrust pad flexibility. *Journal of Engineering Tribology, 230*(7), 872–893.

107. Shao, J. P., Zhang, Y. Q., & Li, P. C. (2007). Static flow simulation of hydrostatic bearing ellipse and sector curve based on FLUENT. *Lubrication Engineering, 1*, 93–95.

108. Zhang, Y. Q. (2007). *Research of flow and temperature fields of hydrostatic bearing based on fluent*. Harbin University of Science and Technology.

109. Shao, J. P., Zhang, Y. Q., Yu, X. D., Qin, B., & Wang, Z. W. (2009). Numerical simulation analysis of sector and circular oil recess temperature field of heavy hydrostatic. *Journal of Hydrodynamics, 24*(1), 120–124.

110. Shao, J. P., Dai, C. X., Zhang, Y. Q., Yu, X. D., Xu, X. Q., & Wang, Y. F. (2011). The effect of oil cavity depth on temperature field in heavy hydrostatic thrust bearing. *Journal of Hydrodynamics, 23*(5), 676–680.

111. Wang, Y. Z., Jiang, D., Yin, Z. W., Gao, G. Y., & Zhang, X. L. (2015). Load capacity analysis of water lubricated hydrostatic thrust bearing based on CFD. *Journal of Donghua University (Natural Sciences), 41*(4), 428–432.

112. Li, X. B., Huang, Y., Li, M., Cheng, T. (2016). Influences on temperature field of a vertical lathe hydrostatic thrust bearing by structural dimension of oil cushion. *Machine Tool & Hydraulics, 44*(21), 128–131.

113. Sun, D. D. (2017). *Optimization research on lubrication performance of the hydrostatic thrust bearing with double rectangular cavity*. Harbin University of Science and Technology.

114. Xiao, J. F., Shen, F., Liu, Z.M. (2017). Numerical simulation study on flow characteristics of a new multi-annular oil chamber. *23rd Annual Meeting of Beijing Mechanics Society*, 51-52.

115. Guo, Y. P., Zhang, Y. Q., Deng, L. Y., Zhang, H.X. (2018). Comparative analysis of temperature rising characteristics of hydrostatic bearing oil film with different cavity structures. *Harbin University of Science and Technology, 23*(4), 55–58.

116. Shao, J. P., Liu, G. D., Yu, X. D., Zhang, Y. Q., Meng, X. L., & Jiang, H. (2018). Effect of recess depth on lubrication performance of annular recess hydrostatic thrust bearing by constant rate flow. *Industrial Lubrication and Tribology, 70*(1), 68–75.

117. Yu, M. B., Yu, X. D., Zheng, X. H., Qu, H., Yuan, T., & Li, D. (2019). Influence of recess shape on comprehensive lubrication performance of high speed and heavy load hydrostatic thrust bearing. *Industrial Lubrication and Tribology, 71*(2), 301–308.

118. Wang, Y. (2021). *Research on cavity effect of high speed and heavy load hydrostatic thrust bearing*. Harbin University of Science and Technology.

119. Tian, Z. X., Guo, M. H., & Cao, H. Y. (2022). Study on influencing factors of dynamic characteristics of annular recess hydrostatic thrust bearing. *Chinese Journal of Engineering Design, 29*(4), 456–464.

120. Markin, D., Mc Carthy, D. M. C., & Glavatskih, S. B. (2003). A FEM approach to simulation of tilting-pad thrust bearing assemblies. *Tribology International, 36*, 807–814.

121. Santos, I., & Kristian, B. (2007). Geometry optimization of hybrid tilting-pad journal bearings. *Proceeding of the ASME/STLE International Joint Tribology Conference, 2007*, 319–321.

122. Shao, J. P., Yang, X. D., Zhou, L. M., Li, H., Zhang, Y., & Jiang, H. (2009). Numerical simulation of integrated deformation of heavy hydrostatic thrust bearing and experimental research. *International Conference on Intelligent Human-Machine Systems and Cybernetics, 2009*, 45–48.

123. Yang, X. D. (2010). *Research on temperature field and deformation field of large-scale constant-current hydrostatic bearing*. Harbin University of Science and Technology.

124. Yu, X. D., Fu, X., Liu, D., Zhou, Q. H., Li, H. H., & Wang, Z. Q. (2015). Thermal deformation of annular recess multi-pad hydrostatic thrust bearing. *Journal of Jilin University (Engineering and Technology Edition), 45*(2), 460–465.

125. Ettles, C. M., López, G. D., & Borgna, H. (2016). Optmized design of a large reversible thrust bearing. *Journal of Tribology, 138*(4), 1701–1709.

126. Yu, X. D., Wu, X. G., Sui, J. L., Sun, D.D., Zhang, Y.Q. (2016). Numerical and experimental study on temperature field of hydrostatic bearing friction pairs. *Journal of Propulsion Technology, 37*(10), 1946–1951.

127. Yu, X. D., Liu, C., Zuo, X., & Zh, Y. Q. (2018). Fluid-thermal-mechanical coupled solution and experiment on deformation of bearing friction pairs in hydrostatic bearing. *Engineering Mechanics, 35*(5), 231–238.

128. Yu, X. D., Zuo, X., Liu, C., Zheng, X., Qu, H., & Yuan, T. (2018). Oil film shape prediction of hydrostatic thrust bearing under the condition of high speed and heavy load. *Industrial Lubrication and Tribology, 70*(7), 1243–1250.

129. Zheng, X. J. (2018). *Study on the thermal characteristics of the static pressure rotary table in extreme working conditions*. Harbin University of Science and Technology.

130. Yu, X. D., Gao, W. C., & Wu, G. P. (2020). Thermal performance characterization of hydrostatic thrust bearing under high speed and heavy load working conditions. *Journal of South China University of Technology (Natural Science Edition), 48*(9), 79–85.

131. Li, X. B., Li, W. X., Chen, X. Y., Li, M., Chen, H., & Yue, X. (2018). Design and performance analysis on heat pipe hydrostatic thrust bearings based on rectangular oil pad. *Industrial Lubrication and Tribology, 70*(7), 1251–1257.

132. Geng, L. (2018). *Dynamic and static characteristics research of hydrostatic thrust bearing under extreme conditions*. Harbin University of Science and Technology.

133. Yu, X. D., Yuan, T. F., Li, D. G., Qu, H., & Zheng, X. (2018). Dynamic characteristics of hydrostatic thrust bearing with double rectangular cavity under extreme working condition. *Chinese Journal of Theoretical and Applied Mechanics, 50*(4), 899–907.

134. Yu, M. B., Yu, X. D., Zheng, X. H., & Jiang, H. (2019). Thermal-fluid-solid coupling deformation of hydrostatic thrust bearing friction pairs. *Industrial Lubrication and Tribology, 71*(3), 467–473.

135. Brecher, C., Baum, C., Winterschladen, M., & Wnnzel, C. (2007). Simulation of dynamic effects on hydrostatic bearings and membrane restrictors. *Production Engineering, 1*(4), 415–420.

136. Stansfield, F. M. (2003). *Hydrostatic bearings for machine tools and similar applications*. The Machinery Publishing.

137. Zhang, B. Z. (2003). *Numerical method of fluid mechanics*. The Machinery Publishing.

138. Osman, T. A., Safar, Z. S., & Mokhtar, M. O. A. (1991). Design of annular recess hydrostatic thrust bearing under dynamic loading. *Tribology International, 24*(3), 137–141.

139. Sui, J. L. (2017). *Research on the tribology behavior of inclinable hydrostatic thrust bearing with self-adaption oil pad*. Harbin University of Science and Technology.

140. Wang, Z. X. (2018). *Study on oil film stiffness performance of high speed and heavy load hydrodynamic and hydrostatic mixed lubrication thrust bearing*. Harbin University of Science and Technology.

141. Yu, X. D., Liu, C., & Zuo, X. (2018). Hydrodynamic compensation of carrying capacity in hydrostatic thrust bearing under extreme working condition. *Journal of Propulsion Technology, 39*(5), 1085–1091.

142. Zuo, X. (2019). *Research on comprehensive lubrication performance of static and dynamic pressure hybrid static pressure bearing*. Harbin University of Science and Technology.

143. Yuan, T. F. (2020). *Study on morphology characteristics of oil film in static and dynamic pressure mixed support*. Harbin University of Science and Technology.

144. Qu, H. (2020). *Temperature characteristics and deformation characterization of adaptive hydrostatic thrust bearing*. Harbin University of Science and Technology.

145. Yu, X. D., Zhan, S. W., Han, F., Wang, F., Sun, F., Huang, D., & Jiao, J. (2021). Deformation of friction pairs of static and dynamic pressure hybrid bearing with tilting oil pad. *Engineering Mechanics, 38*(1), 241–248.

146. Zhou, W. K. (2021). *Research on static and dynamic characteristics of new type oil cushion tilting hydrostatic thrust bearing*. Harbin University of Science and Technology.

147. Razzaque, M. M., & Hossain, M. Z. (2015). Effects of grooving in a hydrostatic circular step thrust bearing with porous facing. *Journal of Tribology, 137*(3), 031703-1–031703-10.

148. Wu, G. P. (2021). *Research on the influence of surface microstructure on friction characteristics of high-speed and heavy-load hydrostatic support*. Harbin University of Science and Technology.

149. Li, J., Ma, J. K., Ding, L. W., & Liu, Z.Y. (2019). Numerically simulating pressure field of oil film in a new hybrid rotary table. *Mechanical Science and Technology for Aerospace Engineering, 38*(12), 1812–1818.

150. Ding, L. W. (2018). *Numerical simulation of flow field and temperature field of the new type hybrid rotary table based on CFD*. Shandong University.

151. Liu, Y. P., Ma, J. K., Chen, S. J., Lu, C.H. (2017). The analysis of new-type hybrid rotary table's carrying-capacity characteristics and structure improvement. *Modular Machine Tool & Automatic Manufacturing Technique, 10*, 6–11.

152. Nie, Y. L., Ma, J. K., Chen, S. J., Tian, Z.H. (2019). Study on oil film force and dynamic characteristics of a new type hybrid rotary table. *Lubrication Engineering, 44*(11), 73–78.

153. Nie, Y. L. (2019). *Study on axial static-dynamic characteristics and circumferential motion stability of the new type hybrid rotary table*. Shandong University.

154. Tian, Z. H., Ma, J. K., Lu, C. H., Chen, S.J., Nie, Y.L. (2019). Parameter optimization of the spiral groove on a novel hybrid rotary table. *Modular Machine Tool & Automatic Manufacturing Technique, 5*, 9–13.

155. Liu, Z. Y., Ma, J. K., & Li, J. (2020). Oil film temperature rise characteristics of a new type hybrid differential rotary table without negative pressure. *Lubrication Engineering, 45*(4), 45–50.

156. Liu, Z. Y. (2020). *Study on the shunt characteristics a new type hybrid rotary table*. Shandong University.

157. Zhu, X. S., Xue, B. Y., & Bei, J. Y. (1990). Essence of rotational error motion and its test and calculating method. *Journal of Shanghai Jiaotong University, 4*, 52–60.

158. Xiong, W. L., Yang, X. B., Lang, L., & Yuan, J. (2009). Review on key technology of hydrodynamic and hydrostatic high-frequency motor spindles. *Journal of Mechanical Engineering, 45*(9), 1–18.

159. Chen, C. H., Kang, Y., Huang, Y. N., Chu, C. H., & Teng, J. T. (2002). The restrictive effects of capillary compensation on the stability of the Jeffcott rotor-hybrid bearing system. *Tribology International, 35*(12), 849–855.

160. Chen, C. H., Kang, Y., Chang, Y. P., Lee, H. H., & Shen, P. C. (2005). Influences of recess depth on the stability of the Jeffcott rotor supported by hybrid bearings with orifice restrictors. *Industrial Lubrication and Tribology, 57*(1), 41–51.

161. Phalle, V. M., Sharma, S. C., & Jain, S. C. (2012). Performance analysis of a 2-lobe worn multirecess hybrid journal bearing system using different flow control devices. *Tribology International, 52*, 101–116.

162. Santos, I., & Watanabe, F. V. (2004). Compensation of cross-coupling stiffness and increase of direct damping in multirecess journal bearings using active hybrid lubrication: Part I: Theory. *Journal of Tribology, 126*(1), 146–155.

163. Haugaard, A. M., & Santos, I. (2010). Stability of multiorifice active tilting-pad journal bearings. *Tribology International, 43*, 1742–1750.

164. Mizumoto, H., Sunahara, T., Yabuta, Y., Arii, S., Fujii, S., Matsumoto, K., & Murakami, K. (2012). Novel diaphragm-control restrictor for precision hydrostatic-bearing spindle. In *4th international conference of Asian-society-for-precision-engineering-and-nanotechnology* (vol. 516, p. 463).

165. Yang, X. D., Wang, Y. Q., Jiang, G. Y., Yan, X. C., & Luo, Y. X. (2015). Dynamic characteristics of hydrostatic active journal bearing of four oil recesses. *Tribology transactions, 58*(1), 7–17.

166. Xiong, W. L., Yuan, S., Hu, C., Wang, J., Fan, L. (2021). The laws and ultimate prediction of rotation accuracy for hydrostatic spindle. *Journal of Mechanical Engineering, 57*(13), 70–82.

167. Singh, N., Sharma, S. C., Jain, S. C., & Reddy, S. S. (2004). Performance of membrane compensated multirecess hydrostatic/hybrid flexible journal bearing system considering various recess shapes. *Tribology International, 37*(1), 11–24.

168. Hu, C., Xiong, W. L., Sun, W. B., & Shuai, Y. (2019). Research on the mechanism of improving hydrostatic spindle rotating accuracy with controllable restrictor. *Journal of Mechanical Engineering, 55*(11), 160–168.

169. Hu, C. (2019). *Research on the mechanism and law of stiffness and accuracy of the hydrostatic spindle with controllable restrictor*. Hunan University.

170. Zhang, S. (2014). *Study of hydraulic bearing of high-speed crankshaft and camshaft grinding machine spindle*. Huazhong University of Science and Technology.

171. Liu, Z. C., Pan, W., Lu, C. H., & Zhang, Y. (2016). Theory research and simulation of hydrostatic spindle axis trajectory based on the piezoelectric thin film differential throttling valve. *Journal of Mechanical Engineering, 52*(21), 71–77.

172. Xia, H., Cui, H. L., & Liu, Y. H. (2018). Analysis on performance of hydrostatic bearing. *Machine Tool & Hydraulics, 46*(4), 84–87.

173. Wang, X. Z., Yu, T. B., Song, Y. H., & Wang, W. S. (2012). Thermal characteristics analysis of liquid hybrid bearing on ultra-high speed grinding. *Advanced Materials Research, 565*, 171–176.

174. Yu, T. B., Wang, X. Z., Guan, P., & Wang, W. (2012). Modal analysis of spindle system on ultra-high speed grinder. *Journal of Mechanical Engineering, 48*(17), 183–188.

175. Chen, D. J., Zhou, S., Bian, Y. H., Fan, J. W., & Zhang, F. H. (2016). Analysis and experimental research of hydrostatic spindle oil film slip phenomenon. *Journal of Mechanical Engineering, 52*(5), 144–153.

176. Pham, V. H., Nguyen, M. T., & Bui, T. A. (2020). Oil pressure and viscosity influence on stiffness of the hydrostatic spindle bearing of a medium-sized circular grinding machine. *International Journal of Modern Physics B, 34*(22–24), 2040156.

177. Abele, E., Altintas, Y., & Brecher, C. (2010). Machine tool spindle units. *Annals of the CIRP, 59*(2), 781–802.

178. Gao, G. Y., Yin, Z. W., Jiang, D., & Zhang, X. (2014). Numerical analysis of plain journal bearing under hydrodynamic lubrication by water. *Tribology International, 75*, 31–38.

179. Chen, D. J., Zhao, Y., & Liu, J. F. (2020). Characterization and evaluation of rotation accuracy of hydrostatic spindle under the influence of unbalance. *Shock and Vibration, 2*, 1–16.

180. Hou, Z., Xiong, W., & Lv, L. (2016). Study on the influence of the journal shape error for hydrostatic spindle rotational error motion. *Journal of Mechanical Engineering, 52*(15), 147–154.

181. Zha, J., Chen, Y. L., & Zhang, P. H. (2017). Relationship between elliptical form error and rotation accuracy of hydrostatic journal bearing. *Industrial Lubrication and Tribology, 69*(6), 905–911.

182. Zhang, P. H., & Chen, Y. L. (2019). Analysis of error motions of axial locking-prevention hydrostatic spindle. *Proceedings of the Institution of Mechanical, 233*(1), 3–17.

183. Fang, C. G., Huo, D. H., & Huang, X. D. (2021). A comprehensive analysis of factors affecting the accuracy of the precision hydrostatic spindle with mid-thrust bearing layout. *The International Journal of Advanced Manufacturing Technology, 114*, 949–967.

184. Yamada, K., Nakao, Y., Suzuki, K. (2013). S131012 Design of water hydrostatic spindle with high stiffness. *The Proceedings of Mechanical Engineering Congress, 13*, S131012-1-S131012-5.

185. Nagasaka, K., Yamada, K., Yamada, Y., Hayashi, A., Nakao, Y. (2014). B27 Influence of water pressure on stiffness of thrust bearing of water hydrostatic spindle. *The Proceedings of The Manufacturing & Machine Tool Conference, 10*, 107–108.

186. Lin, X. W. (2018). *Design of hydrostatic bearing with trapezoidal oil chamber and research on the temperature field based on FLUENT*. Lanzhou University of Technology.

187. Zhang, Y. H. (2020). *Design of oil cavity structure of a radial hybrid bearing under the condition of journal misalignment based on TRIZ*. Zhengzhou University.

188. Zhang, P. F., Zhang, Z. B., & Guo, H. (2021). Kriging model based optimization of conical hybrid bearing. *Modular Machine Tool & Automatic Manufacturing Technique, 2*, 62–65.

189. Guo, S. A., Hou, Z. Q., & Xiong, W. L. (2012). Bearing characteristics study on liquid hybrid bearing based on CFD. *Manufacturing Technology & Machine Tool, 9*, 57–61.

190. Wang, L., & Jiang, S. Y. (2013). Performance analysis of high-speed deep/shallow recessed hybrid bearing. *Mathematical Problems in Engineering, 6*, 1–9.

191. Meng, S. G., Xiong, W. L., & Wang, S. L. (2015). Analytical research on characteristics of deep-shallow journal bearings with orifice restrictors. *Journal of Mechanical Engineering, 51*(22), 191–201.

192. Guo, L., Cao, S., & Hu, J. (2015). Coupling analysis of thermal-dynamics characteristics of high efficiency and precision hybrid spindle. *Mechanical Science and Technology for Aerospace Engineering, 34*(11), 1686–1692.

193. Wang, P., Liu, B. G., Feng, E., Zhao, G. (2017). Oil film bearing characteristics of deep-shallow pockets hybrid bearing. *Applied Technology, 284*, 78–80.

194. Liu, L., Liu, B. G., Wang, P., Shen, H.P., Ding, H. (2019). Analysis of oil film pressure field and temperature field of hydrodynamic and hydrostatic bearing. *Journal of Mechanical & Electrical Engineering, 36*(9), 900–906.

195. Zhang, Y. M., Yu, D. G., & Yang, Q. B. (2018). Oil film characteristics of deep-shallow pocket hybrid bearing. *Journal of Northeastern University (Natural Science), 39*(10), 1490–1494.

196. Liu, L. (2020). *Multi-objective optimal design of ultra-high speed grinding electro-spindle hydrodynamic and hydrostatic bearing structure*. Henan University of Technology.

197. Liu, H. Y., & Li, Q. F. (2021). Simulation of oil film pressure of multi-oil chamber bearing based on FLUENT. *Ship Electronic Engineering, 41*(9), 102–107.

198. Ding, H., & Liu, L. (2021). Multi-objective optimization design of hydro-dynamic-static bearing. *Modern Machinery, 4*, 78–81.

199. Guo, H., Jiang, X. Q., & Zhang, Z. B. (2021). Characteristic analysis of conical hybrid bearing based on multi-objective optimization. *Lubrication Engineering, 46*(11), 1–6.

200. Wei, S. J., Yang, S., Hu, W. W., Wang, J.L., Jia, Q. (2022). Simulation and experimental research on performance of hybrid bearings of precision machine tool electric spindle. *Machine tool & Hydraulics, 50*(10), 82–86.

201. Yuan, S. (2020). *Research on accurate simulation and law of rotation accuracy of hydrostatic spindle with controllable restrictor*. Hunan University.

202. Yamada, K., Nagasaka, K., Yamada, Y., Kurihara, K., Hayashi, A., Suzuki, K., & Nakao, Y. (2015). 10515 Influence of water pressure on stiffness of water hydrostatic spindle (Influence of deformation of bearing for displacement of bearing). In *The proceedings of conference of Kanto Branch* (Vol. 21, pp. 105151–105152).

203. Zhao, C. M., Ma, P., Gong, C. L., Niu, X. (2014). Research on characteristics of the high precision hydrostatic spindle system base on one-way fluid-solid interaction. *Lubrication Engineering, 39*(5), 62–68.

204. Kuznetsov, E., & Glavatskih, S. (2015). Dynamic characteristics of compliant journal bearings considering thermal effects. *Tribology International, 94*, 288–305.

205. Zhang, C. (2016). *Study on the performance of hydrostatic bearing oil clearance by bearing shell-main shaft deformation*. Chongqing University.

206. Tang, S. Y., He, Y., & Wang, Y. Z. (2017). Thermo-fluid-solid coupling analysis and experimental study on hybrid bearing. *Lubrication Engineering, 42*, 59–63.

207. Yin, C. Z., Zhang, L. X., Wang, B. R., Yang, H., Li, X. (2019). Multi-physical field coupling simulation and experimental study on thermal characteristics of hydrostatic spindle. *Lubrication Engineering, 44*(9), 126–135.

208. Yin, C. Z. (2019). *Research and optimization of thermal characteristics of hydrostatic spindle*. China Academy of Engineering Physics.

209. Yang, D. P. (2019). *Analysis on oil film properties of hybrid bearings and experiment rig design*. Harbin Institute of Technology.

210. Du, X. (2019). Parameter design of adjustable oil film clearance hydrostatic and hydrodynamic bearing, precise. *Precise Manufacturing & Automation, 4*, 6–10.

211. Chen, D. J., Zhao, Y., Zha, C. Q., & Liu, J. (2020). Fluid-structure interaction on the dynamic characteristics of the hydrostatic spindle in micro-scale. *Industrial Lubrication and Tribology, 72*(3), 397–403.

212. Chen, R. L., Wang, X. Z., Du, C., Liu, K., Yuan, X.Y. (2020). Research on lubrication model and dynamics performance control of the hybrid bearing with single tilting pad. *Manufacturing Technology & Machine Tool, 7*, 117–121.

213. Wang, X. Z. (2021). *Research on lubrication model of hybrid bearing and rotor dynamics performance considering geometric error*. Xi'an University of Technology.

Guangqiang Shi received the M. E. degree from Tarim University in 2020 and is currently studying for the Ph.D. in mechanical engineering at Harbin University of Science and Technology. The main research directions are hydrostatic bearings, fluid mechanics and microstructure.

Xiaodong Yu Professor, Ph. D, PhD Tutor. Harbin University of Science and Technology, Harbin 150080, China. He received the B. S. degree and M. S. degree in the Mechanical Design and Theory from Yan Shan University in 1992 and Harbin University of Science and Technology in 2003, respectively, PhD degree in the Mechanical Design and Theory from Northeast Forestry University in 2007. Now he is a professor and has published over 120 technical articles on hydrostatic thrust bearing, lubrication theory and numerical research of lubrication performance. His current research interests include lubrication theory and bearing manufacturing.

Shihao Li received the B. E. degree from Harbin University of Science and Technology in 2020 and is currently studying for the M. E. degree in mechanical engineering at Harbin University of Science and Technology. The main research directions are lubrication theory and tribological properties.

Weicheng Gao received the M. S. degree from Harbin University of Science and Technology in 2021 and is currently studying for the Ph.D. in mechanical engineering at Harbin University of Science and Technology. The main research directions are hydrostatic bearings, hydrostatic rest and structural optimization.

Minmin Chen received the B. E. degree from University of Jinan in 2018 and is currently studying for the M. S. degree in mechanical engineering at Harbin University of Science and Technology. The main research directions are hydrostatic bearings, electromechanical-hydraulic integration technology and structural optimization.

Yanan Feng received the M. S. degree from Harbin University of Science and Technology in 2020 and is currently studying for the Ph.D. in mechanical engineering at Harbin University of Science and Technology. The main research directions are hydrostatic bearings, fluid mechanics and electromechanical-hydraulic integration technology.

Ruiming Zhang received the B. E. degree from Jilin Institute of Chemical Technology in 2019 and is currently studying for the M. E. degree in mechanical engineering at Harbin University of Science and Technology. The main research directions are hydrostatic bearings, structural optimization and tribological properties.

Junfeng Wang received the M. S. degree in engineering, a researcher senior engineer, is currently the chairman of Qiqihar Heavy CNC Equipment Corp. LTD.

Jianhua Jiao a senior engineer, received the B. S. degree from Qiqihar University. He is the head of the Outstanding Youth Program of the Natural Science Foundation of Heilongjiang Province, chief engineer of Qiqihar Heavy CNC Equipment Corp. LTD, and a member of the "Touyan" team of Heilongjiang Province.

Wentao Jia received the B. S. degree from Changchun University, and studied for the M.S. degree at Harbin University of Science and Technology, is currently the deputy general manager of Qiqihar Heavy CNC Equipment Corp. LTD.

Ruichun Dai received the B. S. degree in the Mechanical Design manufacture and Automation Major from Northeast Forestry University, is currently the section leader of Qiqihar First Machine Tool Factory Corp. LTD.